International Journal of Greenhouse Gas Control 81 (2019) 44–65

Contents lists available at ScienceDirect

International Journal of Greenhouse Gas Control

journal homepage: www.elsevier.com/locate/ijggc

Potential CO_2 and brine leakage through wellbore pathways for geologic CO_2 sequestration using the National Risk Assessment Partnership tools: Application to the Big Sky Regional Partnership

Tsubasa Onishi[a,b,*], Minh C. Nguyen[a,c], J. William Carey[a], Bob Will[d], Wade Zaluski[e], David W. Bowen[f], Bryan C. Devault[g], Andrew Duguid[h], Quanlin Zhou[i], Stacey H. Fairweather[j], Lee H. Spangler[j], Philip H. Stauffer[a]

[a] Earth and Environmental Sciences Division, Los Alamos National Laboratory, Los Alamos, NM 87545, USA
[b] Department of Petroleum Engineering, Texas A&M University, College Station, TX 77843, USA
[c] Department of Geology & Geophysics, University of Wyoming, Laramie, WY 82071, USA
[d] WRG Subsurface Consulting, Littleton, CO 80123, USA
[e] Schlumberger Canada, Calgary, Alberta, T2G 0P6, Canada
[f] Department of Earth Sciences, Montana State University, Bozeman, MT 59717, USA
[g] Vecta Oil and Gas, The Woodland, TX 77380, USA
[h] Battelle Memorial Institute, Columbus, OH 73201, USA
[i] Energy Geosciences Division, Lawrence Berkeley National Laboratory, Berkeley, CA 94720, USA
[j] Energy Research Institute, Montana State University, Bozeman, MT, 59717, USA

ARTICLE INFO

Keywords:
Geologic CO_2 sequestration
Uncertainty assessment
Risk assessment
Reservoir simulation
Design of experiment

ABSTRACT

Geologic CO_2 sequestration (GCS) has received high-level attention from the global scientific community as a response to climate change due to higher concentrations of CO_2 in the atmosphere. However, GCS in saline aquifers poses certain risks including CO_2/brine leakage through wells or non-sealing faults into groundwater or to the earth's surface. Understanding crucial reservoir parameters and other geologic features affecting the likelihood of these leakage occurrences will aid the decision-making process regarding GCS operations. In this study, we develop a science-based methodology for quantifying risk profiles at geologic CO_2 sequestration sites as part of US DOE's National Risk Assessment Partnership (NRAP). We apply NRAP tools to a field scale project in a fractured saline aquifer located at Kevin Dome, Montana, which is part of DOE's Big Sky Carbon Sequestration Partnership project. Risks associated with GCS injection and monitoring are difficult to quantify due to a dearth of data and uncertainties. One solution is running a large number of numerical simulations of the primary CO_2 injection reservoir, shallow reservoirs/aquifers, faults, and wells to address leakage risks and uncertainties. However, a full-physics simulation is not computationally feasible because the model is too large and requires fine spatial and temporal discretization to accurately reproduce complex multiphase flow processes. We employ the NRAP Integrated Assessment Model (NRAP-IAM), a hybrid system model developed by the US-DOE for use in performance and quantitative risk assessment of CO_2 sequestration. The IAM model requires reduced order models (ROMs) developed from numerical reservoir simulations of a primary CO_2 injection reservoir. The ROMs are linked with discrete components of the NRAP-IAM including shallow reservoirs/aquifers and the atmosphere through potential leakage pathways. A powerful stochastic framework allows NRAP-IAM to be used to explore complex interactions among a large number of uncertain variables and to help evaluate the likely performance of potential sequestration sites. Using the NRAP-IAM, we find that the potential amount of CO_2 leakage is most sensitive to values of permeability, end-point CO_2 relative permeability, hysteresis of CO_2 relative permeability, capillary pressure, and permeability of confining rocks. In addition to demonstrating the application of the NRAP risk assessment tools, this work shows that GCS in the Kevin Dome has a higher probability of encountering injectivity limitations during injection of CO_2 into the Middle Duperow formation than previous studies have calculated. Finally, we estimate very low risk of CO_2 leakage to the atmosphere unless the quality of the legacy well completions is extremely poor.

* Corresponding author.
E-mail address: tsubasa0024@tamu.edu (T. Onishi).

https://doi.org/10.1016/j.ijggc.2018.12.002
Received 4 April 2018; Received in revised form 30 November 2018; Accepted 1 December 2018
Available online 04 January 2019

1. Introduction

Global warming is an environmental issue linked to the rise in global average temperatures because of increases in greenhouse gases such as carbon dioxide (CO_2) and methane in the atmosphere. Geologic carbon sequestration (GCS) has been proposed as a method to mitigate global warming (Metz et al., 2005). Candidate formations for GCS include depleted hydrocarbon reservoirs, unmineable coalbeds and saline aquifers (Bachu, 2000). While saline aquifers are known to have the highest capacity for large scale subsurface storage, GCS in saline aquifers poses certain risks including CO_2 and brine leakage through abandoned wellbores or non-sealing faults into ground water or to the earth surface. Besides the aspect of global warming, leakage of CO_2 and brine can threaten groundwater resources (Keating et al., 2010; Trautz et al., 2012; Wilkin and DiGiulio, 2010).

In an effort to better understand GCS, the US Department of Energy formed partnerships between industry, universities, and national laboratories to explore the viability of this concept in different regions of the United States. The Big Sky Carbon Sequestration Partnership's (BSCSP) Kevin Dome project is one of several Regional Carbon Sequestration Partnership Phase III Development projects with an intent to inject one million metric tonnes (MT of CO_2 into a storage formation while validating site characterization, modeling and monitoring techniques. The target reservoir is the middle Duperow, a Devonian era carbonate (mixed dolostone and limestone) interval of ~100 ft thickness that produced CO_2 in drill stem tests of historic wells near the apex of the dome but contains brine down dip. The original project scope planned to use the gas cap as the CO_2 source and the same reservoir in the down-dip brine leg as the storage target. This approach could provide some unique advantages: 1) wellbore data (logs and core) from the gas cap and brine leg would allow comparison of reactive reservoir rock and caprock exposed to CO_2 over geologic time vs. an engineered storage timescale providing insight on geochemical impacts on injection and storage; and 2) the concept of domes as storage hubs could be tested where CO_2 could be injected for storage and produced for enhanced oil recovery thereby decoupling CO_2 production and utilization rates (http://www.bigskyco2.org/).

In the process of the Kevin Dome site characterization, it was determined that, counter to regional data trends, the targeted storage region had less than 10,000 ppm total dissolved solids (TDS) which means it classifies as an Underground Source of Drinking Water (USDW) by the primary criterion in the Environmental Protection Agency's (EPA) Underground Injection Control (UIC) regulations. The storage reservoir also had significant levels of H_2S and while most well classes allow for exceptions to the 10,000 ppm TDS minimum (e.g. if hydrocarbons or toxic substances are present at high enough levels), Class VI for CO_2 injection does not. Thus the project would be unable to secure a CO_2 injection permit. Nonetheless, valuable samples and data were acquired during site characterization including over 36 sq mi of 3-dimensional, 9-component seismic data, and wellbore data from two wells, one in the brine leg and one in the CO_2 gas cap that include modern log suites and 45 ft of core of reservoir and caprock (the low permeability upper Duperow and the overlying Potlatch anhydrite). The project has been re-scoped to utilize the existing samples and data to contribute to understanding CO_2 storage including the study reported here.

The scale of the BSCSP Kevin Dome project is typical of a GCS field site, and CO_2 injection risk assessment would likely require reservoir models spanning 10 s–100 s of km^2 in areal extent with a vertical extent of well over 1 km. In addition to a model for the injection reservoir, systems of faults, existing wellbores, overlying underground sources of drinking water (USDW), and leakage of CO_2 to the surface need to be considered. Coupled site models incorporating these sub-models are necessary to make predictions about site behavior and to provide insight into site evolution. In a typical workflow, site models are refined as data become available to better simulate actual site behavior with a goal of reducing uncertainty and reducing risks to site operations. Risk proxies can be used to gauge possible impacts without calculating true risk values that require estimates of impacts that are often difficult to quantify. Risk proxies used previously for the Kevin Dome project include CO_2 injectivity; radius of the Area of Review (AoR); CO_2 migration out of the injection horizon; and optimum location of monitoring wells (Dai et al., 2014).

One solution to creating a fully coupled site model is running high-fidelity, multiphase numerical simulations for an entire domain including a storage reservoir, shallow aquifers, wellbores, and faults across large spatial and temporal scales of GCS operation. Although this approach can address complex multiphase flow and trapping mechanisms, it requires fine spatial and temporal discretization to accurately model these complex physics that is usually computationally expensive. In addition, assessing these risks can easily require a large number of numerical simulations to span the many uncertainties and therefore this approach is not computationally attractive. Several (semi-) analytical models are available (Mathias et al., 2011, 2009; Mijic et al., 2014; Nordbotten et al., 2005; Vilarrasa et al., 2013; Zhou et al., 2017). While analytical models provide significant benefits in terms of computational cost, these approaches are limited to, for example, homogeneous media, simple geometry, or incompressible flow that can potentially result in erroneous prediction of plume geometry.

Los Alamos National Laboratory (LANL) initiated a hybrid (numerical plus analytical) system model, CO_2-PENS (Predicting Engineered Natural Systems) (Pawar et al., 2006; Stauffer et al., 2013, 2011; Stauffer et al., 2006) which is an Integrated Assessment Model (IAM) used to determine CO_2 storage risk profiles. This tool was adapted to use as the base IAM for the US-DOE funded National Risk Assessment Partnership and the expanded tool, including contributions from several national laboratories (Carroll et al., 2016; Nguyen et al., 2017a), has been named NRAP-IAM (Pawar et al., 2016). NRAP-IAM simulates CO_2 storage reservoir security using reduced order models that are computationally efficient and allow analysis of the impact of uncertainty on prediction of leakage potential. NRAP-IAM decomposes the problem into interacting discrete components including a storage reservoir, wells, faults, intermediate reservoirs, shallow aquifers and the atmosphere. Each component has assigned properties with a range of uncertainties. For example, the pressure-saturation history of the CO_2 storage reservoir is represented using reduced order models (ROMs) developed from the results of full-physics simulations of CO_2 injection processes (Stauffer et al., 2016). Legacy wells within the area of interest have uncertainties in terms of total number, location, and quality (wellbore integrity) (Harp et al., 2016; Hu et al., 2012; Jordan et al., 2015; Viswanathan et al., 2008). Shallow drinking-water aquifers have uncertainties associated with permeability, porosity and thickness (Carroll et al., 2016; Keating et al., 2010). NRAP-IAM allows the user to explicitly define parameter values where data is available or to use generic properties obtained from the literature. The CO_2 storage system components are linked through potential CO_2 and brine pathways such as legacy wells and unsealed faults. Results of CO_2 migration are calculated in a Monte-Carlo framework in terms of 1) the amount of CO_2 present in the various model components, including reservoir and shallow formations, 2) the areal and volumetric extent of CO_2 plumes in the reservoir and shallow formations, and 3) components potentially impacted by CO_2 migration, such as shallow groundwater wells. The powerful stochastic framework allows NRAP-IAM to be used to explore complex interactions among a large number of uncertain variables and to help evaluate the likely performance of potential sequestration sites.

In the NRAP-IAM framework, the Reservoir Reduced Order Model –Generator (RROM-Gen; King (2016)), is used to convert reservoir simulation outputs from full-physics codes into lookup tables necessary to run the NRAP-IAM for uncertainties in a storage reservoir. RROM-Gen can utilize reservoir simulation data from a number of different simulators such as FEHM (Zyvoloski, 2007), TOUGH2 (Pruess et al., 1999), ECLIPSE (https://www.software.slb.com/products/eclipse),

Petrel (https://www.software.slb.com/products/petrel), CMG Software (https://www.cmgl.ca/software), and STOMP (White et al., 1995). RROM-Gen extracts permeability, porosity, elevation, CO_2 saturation, dissolved CO_2 concentration, temperature, and pressure from the layer with the highest CO_2 concentrations in the injection reservoir to use as input for risk analysis in NRAP-IAM. Bilinear interpolation is performed to map full-physics calculations and input data on these reservoir properties onto the 100 × 100 grid used within the NRAP-IAM. The interpolated sets of properties are Reduced Order Models (ROMs) that provide uncertain parameters for the storage reservoir (Fig. 1).

Viswanathan et al. (2008) and Stauffer et al. (2009) applied CO_2-PENS to CO_2 sequestration scenarios in synthetic cases including a depleted oil reservoir and saline aquifer. In these studies, CO_2-PENS had multiple options for leakage through wellbores including analytical wellbore leakage modules created by the Princeton-CMI group (Nordbotten et al., 2008) and the use of a multiphase-numerical simulator Finite Element Heat and Mass-Transfer (FEHM) (Zyvoloski, 2007). The first option was validated with CO_2 sequestration scenarios in simple homogeneous cases over 2500 days by comparing with numerical simulation results using ECLIPSE (Nordbotten et al., 2008). Their comparisons show deviations in early time because of numerical dispersion in ECLIPSE and good agreement at late time. However, there is no guarantee that the analytical solution can maintain accuracy after the short period (2500 days) because assumptions in the analytical solution may not be valid over hundreds of years which is a typical CO_2 storage and monitoring scenario. While analytical models may be applicable to simple scenarios, they may not be capable of field case studies involving complexities such as heterogeneous permeability distributions. Although accurate, the second option using FEHM to model wells can be computationally expensive if uncertainties are high and a large number of simulations are needed.

Jordan et al. (2015) and Harp et al. (2016) developed wellbore leakage ROMs using a Design of Experiment (DoE)-based method. In their approach, the Multivariate Adaptive Regression Splines (MARS) algorithm (Friedman, 1991) took as input thousands of FEHM multiphase numerical simulations and was used to build the surrogate models (wellbore leakage ROMs). The DoE-based workflow provides benefits in terms of computational efficiency while overcoming shortcomings of analytical models. A similar workflow has been proposed and applied in several studies including subsurface model calibration (Bhark and Dehghani, 2014; Li et al., 2018) and CO_2 WAG optimization (Olalotiti-Lawal et al., 2018).

Jordan et al. (2015) implemented the wellbore leakage ROMs into CO_2-PENS and used underlying reservoir simulations from the Kimberlina site in central California with several simplifications (Birkholzer et al., 2011). A hypothetical set of five legacy wells were used in the application. Wellbore permeabilities were sampled from a random distribution and 54 full reservoir simulations of CO_2 injection into the Kimberlina reservoir were conducted, and the reservoir simulation results were converted into lookup tables and sampled using uncertain parameters in the storage reservoir.

Although hypothetical, this application showed the utility of the wellbore ROM in being able to quantify the CO_2 and brine leakage risks quickly. However, the sampling method in NRAP-IAM still remains a challenge: the number of numerical simulations required in this approach increases exponentially corresponding to the number of uncertain parameters. Specifically, the logic used in the Kimberlina example requires a minimum of 3^N simulations, where N is the number of uncertain parameters and 3 corresponds to low, base and high values spanning the range of each parameter in a simple box design. There are three uncertain parameters including permeability, pore compressibility, and porosity in the Kimberlina example (Birkholzer et al., 2011), with 6 levels given to the most sensitive, reservoir permeability (Jordan et al., 2015). Thus the number of reservoir simulations required is $6 \times 3 \times 3 = 54$. Although this approach is faster than running numerical simulations for an entire domain including a storage reservoir,

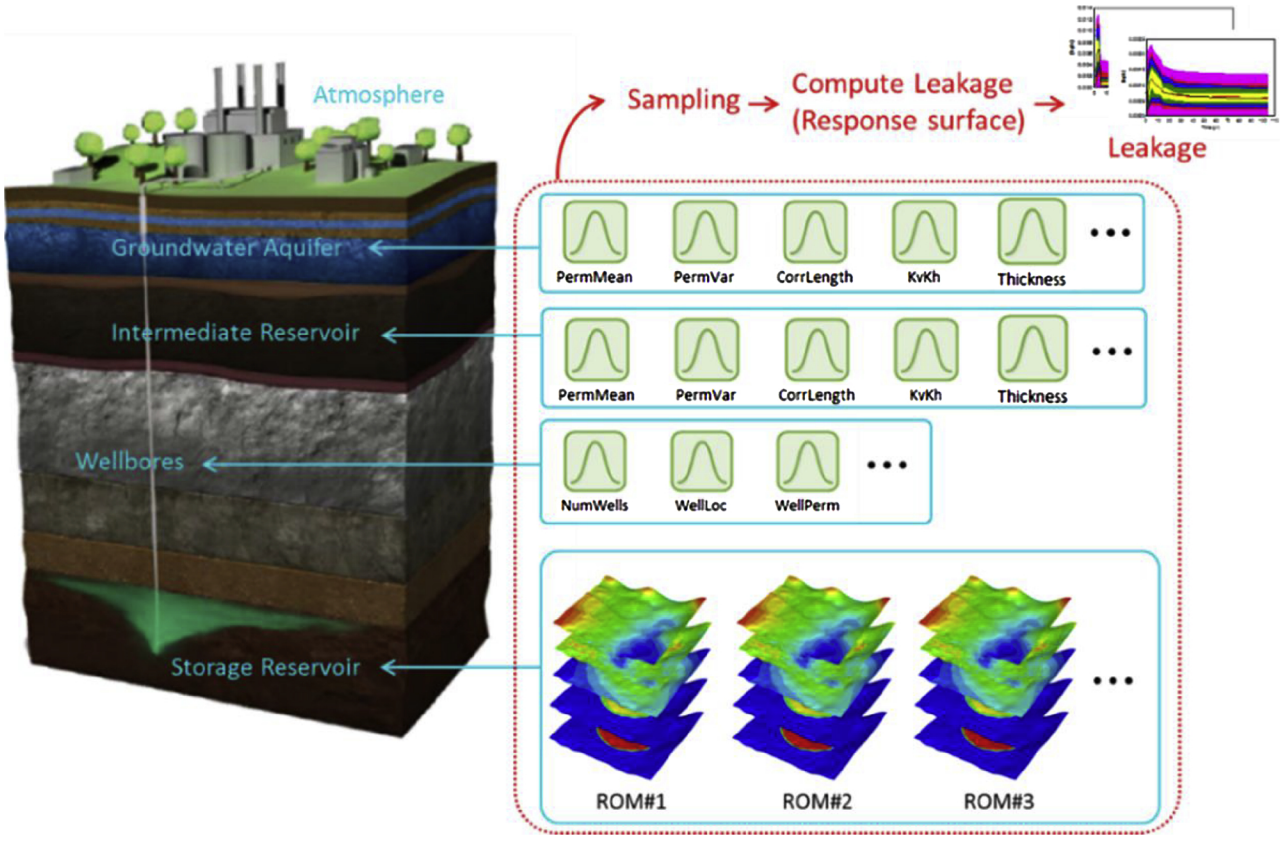

Fig. 1. An illustration of NRAP-IAM: discrete components and corresponding uncertain parameters.

shallow formations and legacy wells, it can be computationally prohibitive in field case applications because there are usually more than three significant uncertainties (e.g., relative permeability (Yoshida et al., 2016) and capillary pressure) and a single simulation can take days. A number of simulation studies and uncertainty quantifications of GCS have been done (Bao et al., 2013; Barrufet et al., 2010; Birkholzer et al., 2011; Dahle et al., 2009; Dai et al., 2014; Harp et al., 2016; Jordan et al., 2015; Nguyen et al., 2017b, c; Olalotiti-Lawal, 2018). However, these only focus on a storage reservoir or include wellbore leakages but with a limited number of uncertain parameters.

Consequently, in this paper we develop a new workflow in which we employ the Latin Hypercube Sampling (LHS) parameter sampling method to generate realizations of numerical simulations for a storage reservoir. LHS is a stratified-random procedure and provides an efficient way of sampling parameters from their distributions (Iman and Conover, 1980; McKay et al., 1979). Unlike random sampling, LHS ensures a full coverage of the range of each parameter by maximally stratifying each marginal distribution. Fewer numerical simulations are required to cover the same range of uncertainties in the developed workflow compared to previous approaches. Or, with the same number of numerical simulations, the LHS approach can investigate more parameters. The new workflow allows NRAP-IAM to be used to perform risk assessment for field scale applications using fewer underlying reservoir simulations resulting in lower computational burden.

To demonstrate the new workflow, this paper presents the first application of the newly released, online, NRAP toolset to a Phase III Regional Carbon Sequestration Partnership dataset. We apply NRAP-tools to a fractured saline storage aquifer located at Kevin Dome in Montana. Data included in the analysis include a 3-D seismic survey, boreholes in the region that penetrate the proposed Big Sky injection horizon, hydraulic testing on the proposed injection well, core analysis and permeability testing, site topography, and groundwater chemistry. Using the Schumberger reservoir simulator, ECLIPSE, we generate simulations of CO_2 injection to explore uncertainty analysis within the NRAP-IAM tool. We investigate a variety of uncertain reservoir parameters including permeability, porosity, relative permeability, hysteresis of relative permeability, capillary pressure, fracture distribution, and salinity of the aquifer. Sensitivity of the NRAP-IAM model results for leakage of both brine and CO_2 are used as criteria to down-select to six primary uncertain variables. These six variables are then used to generate a set of 50 LHS reservoir simulations. The reservoir simulations are extracted into lookup tables and used as input to the NRAP-IAM where leakage uncertainty distributions are generated. We also present estimates of the mass of CO_2 that could be injected during a four-year period at this site and compare results from the new method with previous injection calculations based on regional geological heterogeneity. Finally, convergence of the results with increasing number of NRAP-IAM simulations is discussed.

2. Site description

The Big Sky Carbon Sequestration Partnership (BSCSP) has investigated Kevin Dome, located in Toole County, north-central Montana, and its naturally occurring CO_2 as an analog for carbon storage and as a potential site for additional storage of anthropogenic CO_2. Detailed site characterization, laboratory core studies, well tests, and geologic/geophysical models coupled with operational data have deepened our understanding of the use of site characterization data for predicting geologic system performance. Additionally, this work has improved our understanding of the largest naturally occurring trap of CO_2 in the northwestern United States.

2.1. Reservoir geology

Kevin Dome is a large structural dome formed as a culmination along the Sweetgrass Arch (Fig. 2). The dome covers approximately 700 square miles (1800 square kilometers) at the Devonian Duperow stratigraphic level with approximately 750 feet (229 m) of structural relief. Naturally occurring CO_2 has been documented from several oil and gas wells that have tested the Duperow formation over the past 50 years, but the volume, continuity of the trapped gas, and circumstances of its entrapment have been poorly understood. This dome is integral to trapping oil, natural gas and CO_2 (Fig. 3) and has produced oil and natural gas since its discovery in 1922. Naturally occurring CO_2 is

Fig. 2. Tectonic map of Montana shows Kevin Dome as a large structural closure along the Sweetgrass Arch in north-central Montana (Vuke et al., 2007).

trapped in two major dolomite porosity zones within the Devonian Duperow formation. Oil and natural gas are trapped in shallower limestone and sandstone reservoirs (Fig. 3).

The primary objective of the Big Sky Carbon Sequestration Partnership Phase III project was to extract up to 1 million metric tons of CO_2 from the naturally occurring CO_2 reservoir in the Duperow formation and re-inject it into the brine-filled portion of the Duperow formation at the flank of Kevin Dome (Fig. 3). This project was to demonstrate that the target formation and other analogous formations are viable and safe targets for sequestration of a large fraction of the region's CO_2 emissions. The success criteria for the project would have been to safely inject CO_2 into the storage formation and through models and monitoring establish permanence of storage in the reservoir. The research objectives were to improve the understanding of injectivity, capacity, and storativity in a regionally significant formation.

After extensive efforts by BSCSP, the objective to extract up to 1 million metric tons of CO_2 from the naturally occurring CO_2 reservoir in the Duperow formation and re-inject it into the brine-filled portion of the Duperow formation proved to be unachievable for two reasons: (1) although the natural CO_2 was present as expected, BSCSP was unable to produce the CO_2 in large quantities due to phase transitions of the CO_2 in the reservoir; and (b) the total dissolved solids (TDS) of the brine in the targeted injection formation (Duperow) is less than 10,000 ppm, which is lower than the TDS allowed (no exceptions) for carbon storage under U.S. EPA UIC Class VI injection rules. Neither of these outcomes were predicted from pre-characterization data. Given that the original objective of the BSCSP Phase III project cannot be achieved, the primary objective of the project has been revised to maximize the value of the existing data to DOE's Carbon Storage Program.

2.2. Measured data

2.2.1. Seismic data

Given the anticipated presence and importance of natural fracturing in the targeted Duperow formation, the partnership acquired a multicomponent 3D seismic survey to characterize faulting, natural fractures and porosity heterogeneity in the Duperow. The 9 component 3-dimensional (9C-3D) seismic survey was acquired over three winter field seasons using both shear-wave vibrators and conventional P-wave vibrators. The chosen survey design was a relatively dense, symmetrically sampled orthogonal layout with equal shot and receiver intervals of 110 feet. The corresponding shot and receiver line intervals were 880 and 660 feet respectively. The rectangular recording spread comprised 12 receiver lines, each having 96 channels, which delivered a very good azimuth and offset distribution for inversion of the data for both azimuthal anisotropy parameters and quantities reliant on high-quality long offset information from the horizontal and vertical shear wave (SH and SV) datasets such as density. Each receiver group consisted of a single digital three-component MEMS sensor augured into the ground with dedicated hand drills.

The first phase of the survey comprised the acquisition of approximately 8.5 square miles of 9C-3D data from January to March 2012. The second phase, acquired in the Winter of 2012/2013, resulted in the addition of 19 square miles of data and the final field season in the Winter of 2013/2014 completed data acquisition, resulting in a final survey area of approximately 36 square miles. Notable challenges during acquisition included both extremely cold and warm weather and the ensuing freeze/thaw cycles that greatly slowed field operations, as well as an unexpectedly large number of archeological sites, which had to be delineated and avoided by the seismic acquisition crew.

Data processing for each mode included the traditional steps of geometry assignment and trace edits; compression (P) and shear (S) wave refraction statics using a general linear inversion (GLI) technique; eigenimage ground roll attenuation followed by conventional residual statics and velocity analysis; final noise attenuation in the cross-spread domain; and prestack time migration. Additional steps specific to the multicomponent data included source and receiver rotation (only receiver rotation in the case of the P, S data) and polarization analysis to

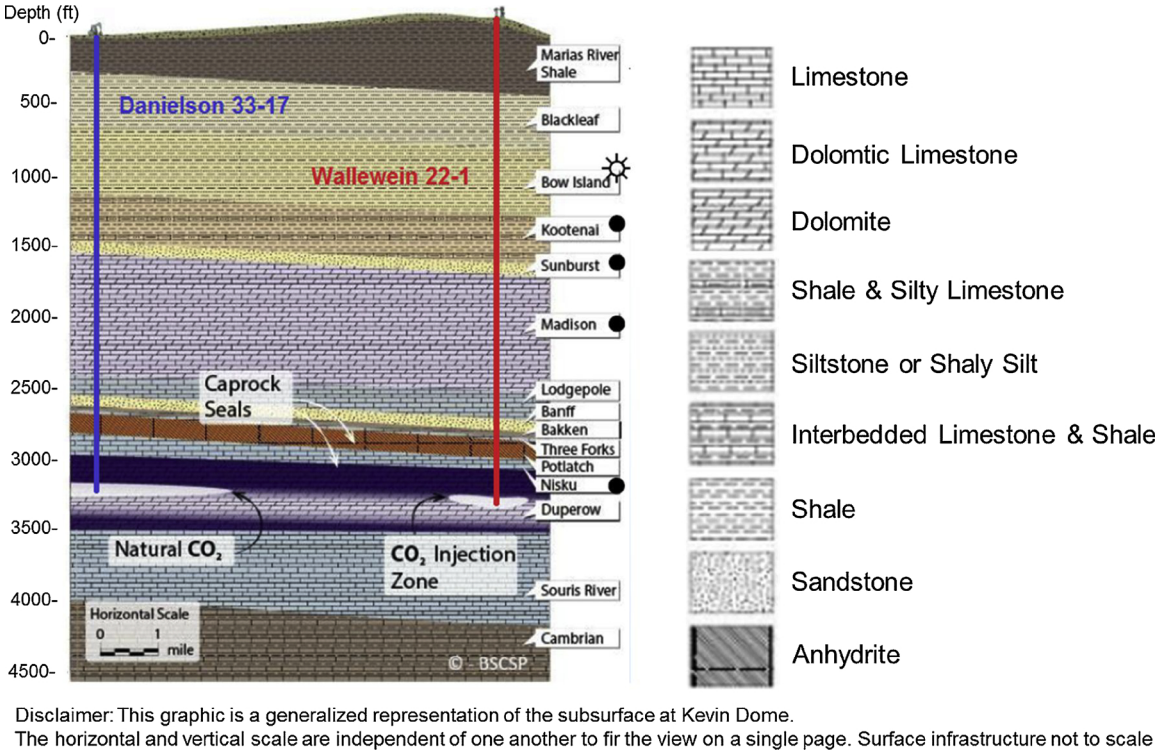

Fig. 3. Schematic cross-section showing the original technical approach that was envisioned for the project. Two principal wells were drilled to provide data for reservoir and site characterization, and to test production potential for CO_2 from the Duperow Fm. (Danielson 33-17 well) and to test potential injectivity (Wallewein 22-1 well).

determine the appropriate anisotropic symmetry system for further processing. Apart from a small area in the northeastern portion of the survey, no measurable azimuthal anisotropy was observed on the shear data, so further processing for the SH, SV, and PS data was performed in a radial-transverse frame after layer stripping the shallow anisotropy observed in the area that did possess azimuthal anisotropy. The PS dataset also required common conversion-point binning due to the asymmetric raypaths characteristic of this mode.

After processing, each individual mode was interpreted for structure and amplitude variations corresponding to changes in rock properties in the overburden and target section. An essential part of the interpretation included a joint inversion of the P data with all of the multi-component data to generate bandlimited P and S impedance and density volumes on the P time scale (Clochard et al., 2018). These datasets were depth converted with depth structure maps created by integrating well tops with their corresponding seismic events at the Bow Island, Sunburst, Potlach, mid-Duperow porosity zone, and Souris River horizons and the resulting 3D seismic volumes were used to constrain the reservoir model built for the project.

2.2.2. Well data

Two wells, the Danielson 33-17 (the first of several proposed production wells to supply CO_2 for the project) and the Wallewein 22-1 (a characterization and monitoring well near the proposed injection site) were drilled to depths below the base of the Duperow formation. The wells were cored in the major Duperow reservoir porosity zone and in primary and secondary caprock seals, and were logged with a detailed suite of tools including gamma ray, neutron porosity, total porosity, effective porosity, neutron magnetic resonance, and other physical variables. An extensive well testing program was implemented in both wells to test reservoir and fluid properties. It was discovered that CO_2 could not feasibly be produced from Danielson 33-17 and the salinity was too low in the middle Duperow formation to be able to obtain a Class VI UIC permit from EPA.

A step-rate injection and pressure fall-off test was conducted by Northern Lights Energy Company and Sanjel on the Wallewein 22-1 well in Toole County, Montana, from March 18, 2015, to March 27, 2015. Tandem electronic quartz gauges were run into the well on March 18, taking gradient stops every 300 feet going into the well. Gauges were set at 4019 ft, and injection of 3% NaCl water began on March 19, 2015, at 09:57 a.m. After completion of all testing, gradient stops were also taken every 300 ft while coming out of the well. Due to operational difficulties with the flowmeter, the injection rates for days 2 and 3 were initially reported to be -854 barrels of water injected per day (bwipd) on day 2, and a final rate of -2000 bwipd on day 3. It was subsequently determined that day 2 and 3 rates were incorrect, thus, it was believed that determining the average injection rate based on volumes pumped would be most accurate. Therefore, for day 2 of injection, an average injection rate of 664 bwipd was used for a pumped volume of 225 barrels (bbls), and for day 3, an average injection rate of 686 bwipd was used for a pumped volume of 248 bbls. After injection, the final fall-off period was extended to 135 h. This pump test data were calibrated into the reservoir model by tuning permeability and porosity (Onishi et al., 2017).

3. Model description

This section presents descriptions of the reservoir simulation model and the risk analysis tools including NRAP-IAM and RROM-Gen.

3.1. Reservoir simulation model

We built a reservoir simulation model based on the measurement and the calibration of the previously conducted pump test data and carried out all simulation runs using the ECLIPSE. A sector model of the field (Fig. 4) was extracted with $69 \times 69 \times 22$ grid discretization with average cell dimensions of $152.4 \times 152.4 \times 3.0$ m (injection zone) based on the radius of investigation which is an analytical function estimating propagation distance of the peak pressure disturbance for an impulse source or sink (Lee, 1982). It is found that the radius of investigation over 104 years (injection: 4 years + post injection: 100 years) based on parameters in the base case (Table 4) is roughly 1300 (m) which is smaller than the distance between the injector and the boundary of our sector model (~5258 (m)). This radius can be larger depending on reservoir properties (e.g., permeability distribution) that will be tuned in the next sections for risk assessment. Through the risk assessment, it is confirmed that size of the sector model is large enough even with reservoir properties resulting in larger CO_2/pressure plume (e.g., high permeability, high CO_2 end point relative permeability, etc.). These will be further discussed in the following sections. Note that the concept of

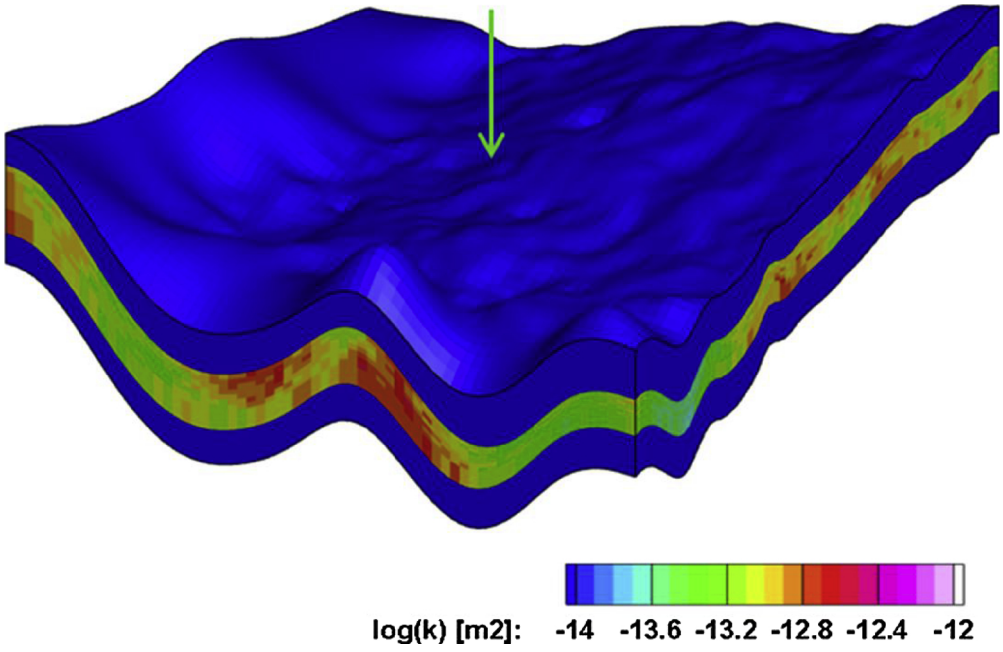

Fig. 4. Permeability distribution of the reservoir simulation model with the injector (Wallewein 22-1) in the middle of the domain.

radius of investigation can be generalized to heterogeneous media using a high frequency asymptotic solution of the diffusivity equation (Iino et al., 2018; Vasco and Datta-Gupta, 2016). In our application, however, the reservoir is slightly heterogeneous and therefore estimates from the radius of investigation are a good approximation. We have compared simulation results between the full model and the sector model and found good agreement validating the use of the smaller sector model.

The geologic model includes a low permeability caprock and basement as part of the CO_2 storage system. The caprock and the basement were upscaled into single layers with average thickness of 60 m. Geological data described above show the existence of fractures with a relatively low permeability contrast between fracture and matrix. A dual-porosity dual-permeability model (Blaskovich et al., 1983; Warren and Root, 1963) was therefore adopted to model fractures because matrix-matrix interactions are important, and yet knowledge of fracture distributions is too limited for use of discrete fracture models (Chen et al., 2018; Noorishad and Mehran, 1982; Hyman et al., 2015; Li and Lee, 2006; Monteagudo and Firoozabadi, 2004).

The fluids modeled in this study using the CO2STORE facility in ECLIPSE for CO_2 storage in the saline aquifer are described by aqueous, gaseous and solid phases, with three components: water (H_2O), carbon dioxide (CO_2), and salt (NaCl) and it is assumed that the system is isothermal (Pruess and Garcia, 2002). Mutual solubilities of CO_2 and H_2O are calculated to match experimental data for typical CO_2 storage conditions (Spycher and Pruess, 2005), based on fugacity equilibrium between water and a CO_2 phase. Henry's law is used to calculate aqueous fugacity; while CO_2 fugacity is calculated using a modified Redlich-Kwong equation of state (Redlich and Kwong, 1949). The gaseous density is obtained by the modified Redlich-Kwong equation of state, in which the attraction parameter is temperature dependent (Spycher and Pruess, 2010). The CO_2 gaseous viscosity was computed based on results from Vesovic et al. (1990) and Fenghour et al. (1998).

In our approach, the Corey equations (Corey, 1954) were applied for relative permeability curves:

$$k_{r,CO2} = k^0_{r,CO2}\left(\frac{S_{CO2} - S_{CO2,ir}}{1.0 - S_{CO2,ir} - S_{brine,ir}}\right)^m \quad (1)$$

and

$$k_{r,brine} = k^0_{r,brine}\left(\frac{S_{brine} - S_{brine,ir}}{1.0 - S_{CO2,ir} - S_{brine,ir}}\right)^n \quad (2)$$

where $k^0_{r,l}$ is the end-point relative permeability of phase l, S_l is the saturation of phase l, $S_{l,ir}$ is the irreducible saturation of phase l, and m and n are the curvature exponents of CO_2 and brine relative permeabilities. Straight-line relative permeability curves are commonly used in dual continuum models (Romm, 1966) for fracture relative permeability functions. However, it has been experimentally and numerically shown that the straight-line relative permeability curves are not always valid (Fourar et al., 1993; Pieters and Graves, 1994). Therefore, we follow previous simulation studies at this site (Zhou, 2013), in which non-idealized relative permeability curves are used for fracture relative permeability. Table 1 provides a summary of parameters used in Eqs. (1) and Eq. (2) following Pruess and Garcia (2002) and Zhou (2013).

The capillary pressure model used in this work is the van Genuchten (1980) model:

$$P_c = P_0\left((S^*)^{-\frac{1}{\lambda}} - 1.0\right)^{1.0-\lambda} \quad (3)$$

where P_0 is the strength coefficient, λ is the pore size distribution index, and the normalized brine saturation S^* is given by

$$S^* = \frac{S_{brine} - S_{brine,ir}}{1.0 - S_{brine,ir}} \quad (4)$$

Table 2 presents parameter values in Eqs. (1) through (4) for the base case following Pruess and Garcia (2002) and Zhou (2013). Note that the same capillary pressure curves are used in the fracture and matrix domain for the base case.

The model consists of a single injection well located in the center of the storage formation. The well, assumed to be connected to all layers in the injection zone, has a radius of 0.07 m Zhou (2013) and injects supercritical CO_2 with a constant temperature of 34.4 °C and bottom-hole pressure (BHP) control of 18.5 MPa which is based on the hydro-fracture limit for the Duperow formation (Dai et al., 2014). We applied a pore volume multiplier of 3000 in lateral boundary cells to mimic a continuous aquifer which is essentially equivalent to a constant pressure boundary (Juanes et al., 2006), while no-flow boundary conditions were applied to top and bottom boundaries. Initial temperature and pressure were set at 34.4 ° C and 10.0 MPa at the top of the injection zone (Zhou, 2013) based on the geothermal gradient and hydrostatic pressure gradient. The initial condition implies that injected CO_2 will be in a supercritical state in the reservoir. The CO_2 injection period lasts for 4 years and the CO_2 plume is monitored over a period of 100 years post-injection that is a sufficient duration for the system to be at equilibrium as shown by the calculated reservoir pressure evolution. Note that values for some of parameters presented in this section such as relative permeability and capillary pressure related parameters are values for the base case and will be tuned in the following sections for sensitivity analysis and risk assessments. In our application, we inject CO_2 at the maximum bottom-hole pressure permitted without damaging the reservoir. As a result, the amount of CO_2 injected varies depending on the reservoir properties. This will be further discussed in the following sections.

3.2. Risk assessment tools

3.2.1. RROM-Gen

RROM-Gen is a tool to convert numerical reservoir simulation outputs into the lookup table input format for NRAP-IAM (100 × 100 lookup bins). The workflow of the RROM-Gen is:

1 Determine a layer from the full-physics model in the injection zone containing the highest CO_2 concentrations (typically the uppermost layer)
2 Extract permeability, porosity, elevation, pressure, temperature, and CO_2 concentrations of the layer from the reservoir simulation outputs
3 Bilinear interpolation to the properties from the step 2 and map them onto a 100 × 100 grid used by NRAP-IAM as a simplified representation of the storage system

The procedures above are performed for every time step for

Table 1
Parameters for relative permeability model (from Zhou, 2013).

Parameter	Values
Fracture	
End-point CO_2 relative permeability, k^0_{r,CO_2} (-)	0.50
End-point brine relative permeability, $k^0_{r,brine}$ (-)	0.15
Irreducible CO_2 saturation, $S_{CO_2,ir}$ (-)	0.10
Irreducible brine saturation, $S_{brine,ir}$ (-)	0.30
Exponent for CO_2 relative permeability, m (-)	2.0
Exponent for CO_2 relative permeability, n (-)	5.0
Matrix	
End-point CO_2 relative permeability, k^0_{r,CO_2} (-)	0.30
End-point brine relative permeability, $k^0_{r,brine}$ (-)	0.05
Irreducible CO_2 saturation, $S_{CO_2,ir}$ (-)	0.25
Irreducible brine saturation, $S_{brine,ir}$ (-)	0.30
Exponent for CO_2 relative permeability, m (-)	2.0
Exponent for CO_2 relative permeability, n (-)	5.0

Table 2
Parameters for capillary pressure model (from Zhou, 2013).

Parameter	Values
Strength coefficient, P_0 (bar)	0.30
Exponent, λ (-)	0.457
Irreducible brine saturation, $S_{brine,ir}$ (-)	0.30
Maximum capillary pressure (bar)	5.0

dynamic data. An example of the RROM-Gen results for a single realization of the Kevin Dome is presented in Fig. 5

In our application, it is found that the top layer of the injection zone in the fracture domain has the highest CO_2 concentrations and is therefore selected as a representative layer. The interpolated sets of properties, RROMs, will be used as uncertain parameters for the storage reservoir in NRAP-IAM and linked through legacy wells to shallower formations and the atmosphere Fig. 1. It is informative to mention that this assumption (a single layer as a representative layer) might overestimate CO_2 and brine leakage compared to the three dimensional full numerical simulation results, however, it is a good approximation for conservative risk assessment purposes.

3.2.2. NRAP-IAM

The NRAP-IAM is a tool to simulate CO_2 storage reservoir security using ROMs that are computationally efficient and allow analysis of the impact of uncertainty on prediction of leakage potential. The NRAP-IAM decomposes the problem into discrete components including a storage reservoir, wells, faults, intermediate reservoirs, shallow aquifers and the atmosphere. Each component has assigned properties with a range of uncertainties and the compartments are linked through potential leakage pathways such as legacy wells and faults. In the Big Sky application, the regional geology includes permeable shallow formations including the Sunburst and Banff (sandstone) and the Madison (dolomitic limestone) (Figs. 3 and 6 (a)). The Madison formation is known as a potential USDW (Kirk, 2002), and its properties are available from previous studies, such as the Thayer (1983) investigation of porosity and permeability in the formation based on well test data. Unfortunately, there is little prior knowledge available for the other two formations. As a result, generic values (Lupe and Ahlbrandt, 1975) are used for the other two formations. Uniform values are used for all gridblocks (100 × 100) in all shallow formations because of the lack of data. In addition, we have prior knowledge for 5 legacy wells penetrating the injection zone (Fig. 6**(b)**) and approximately 45 wells penetrating the shallow formations. Information on wellbore integrity (i.e., permeability of the external annulus) of these wells is not available.

To determine the most important process and parameters related to aquifer impacts, we run the NRAP-IAM and compare CO_2 and brine leakage between cases varying shallow formation rock properties and wellbore integrity. We find that wellbore integrity is more significant than the properties of the shallow formations and conclude that the use of uniform properties for the shallow formations is reasonable. Static properties used in the NRAP-IAM are summarized in Table 3. These data and the RROMs obtained from the RROM-Gen are assigned into each discrete component in the NRAP-IAM. Then, the NRAP-IAM samples N sets of parameters from each component including the atmosphere, shallow formations, the storage reservoir (RROMs), and the legacy wells, where N is the number of Monte-Carlo samples. The CO_2 and brine leakage are then computed for all samples using the wellbore leakage ROMs (response surface) based on thousands of multiphase numerical simulations using FEHM (Jordan et al. (2015); Harp et al. (2016). Each Monte-Carlo realization simulates performance of the CO_2 storage site over 104 years, which includes 4 years of CO_2 injection with BHP control and 100 years of post-injection relaxation and is consistent with the duration in the reservoir simulation.

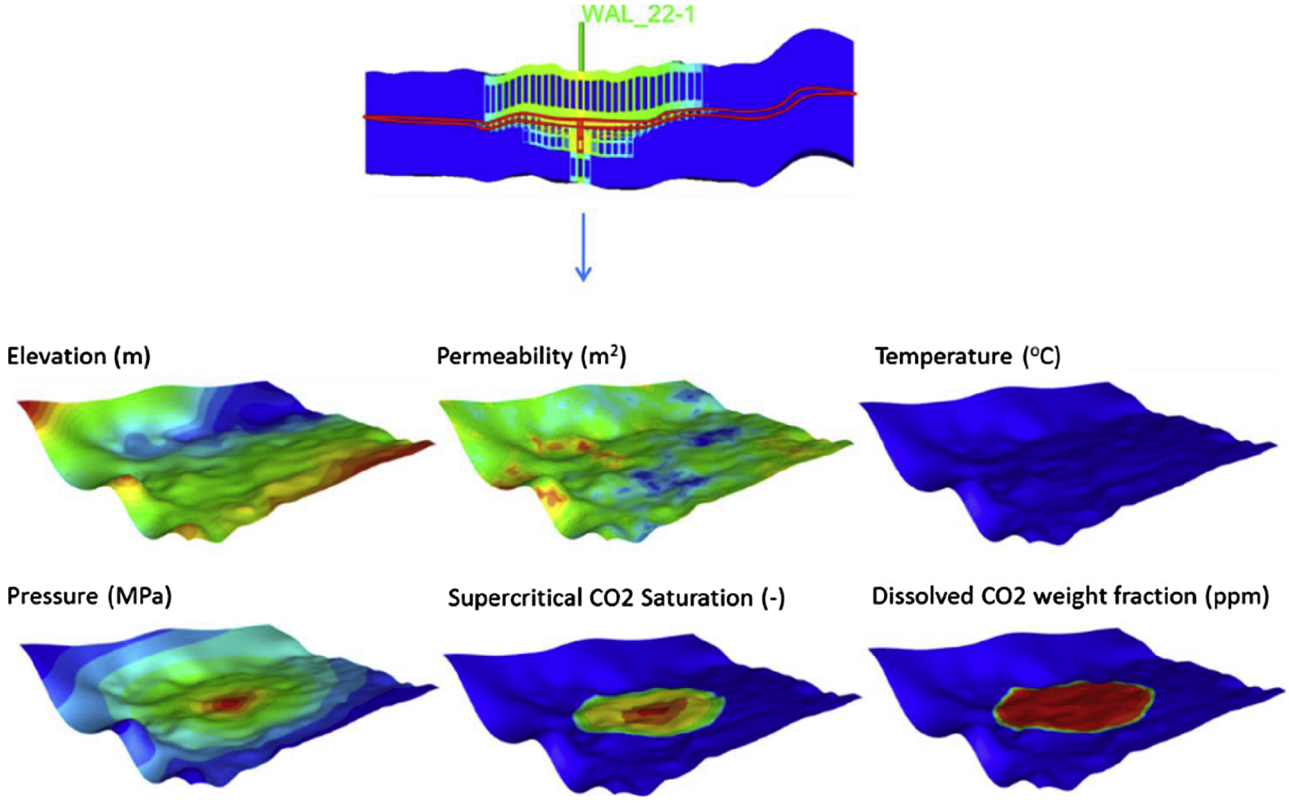

Fig. 5. Extraction of model results for building ROMs using RROM-Gen. The parameters are extracted from the layer outlined in red in the top figure (For interpretation of the references to colour in this figure legend, the reader is referred to the web version of this article).

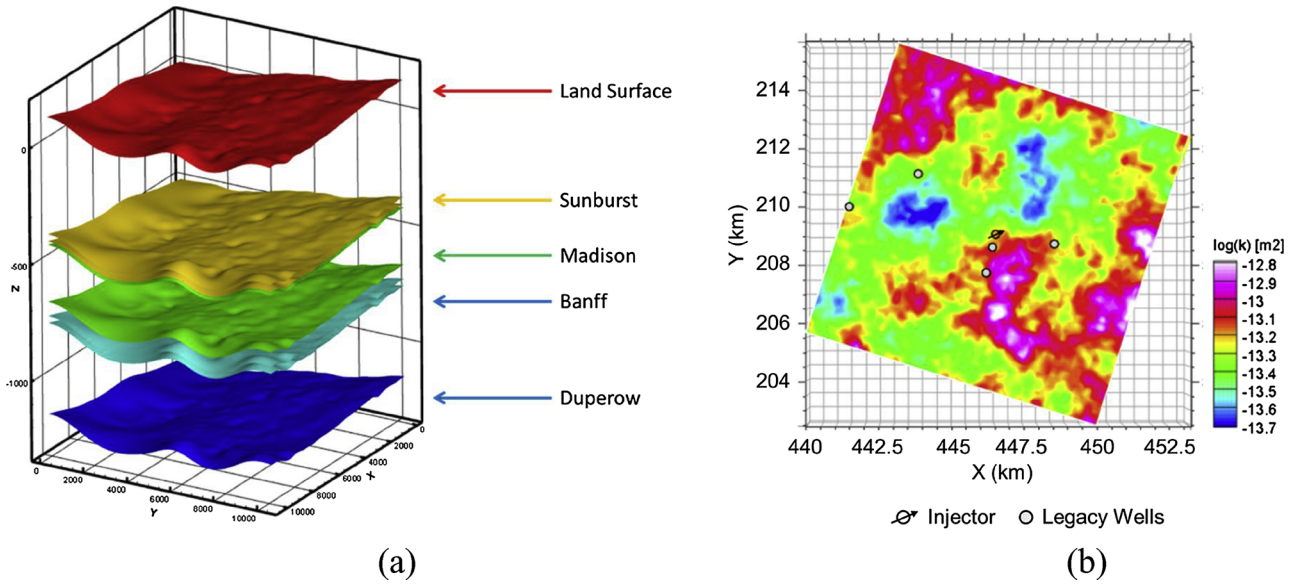

Fig. 6. Shallow permeable formations and legacy well locations: (a) shallow permeable formations (b) legacy well locations in the Middle Duperow, top view (a single injector at center and 5 sparse legacy wells).

Table 3
Parameters for NRAP-IAM.

Parameter	Values
Sunburst	
Thickness, (m)	30.0
Permeability, (m^2)	9.9e-14
Porosity, (-)	0.15
Madison	
Thickness, (m)	240.0
Permeability, (m^2)	9.9e-15
Porosity, (-)	0.15
Banff	
Thickness, (m)	30.0
Permeability, (m^2)	9.9e-14
Porosity, (-)	0.15
Wells	
Number of wells in the injection zone, (-)	5
Number of wells in shallow formations, (-)	45
Wellbore cement effective permeability, (m^2)	Sample from a probability distribution*

*Log normal distribution (μ = 9.5e-15(m^2), σ = 1.18e-13(m^2)).

4. Risk assessment

Here we present the methodology and results of the risk assessment for GCS in the Kevin Dome site using the reservoir simulation and the NRAP tools discussed in the previous sections. The workflow consists of three primary elements: 1) Sensitivity analysis; 2) reservoir simulation; 3) NRAP-IAM simulation (Fig. 7). Details of each step will be discussed in following subsections.

4.1. Sensitivity analysis

4.1.1. Methods

The first step of the sensitivity analysis is to identify the key performance parameters that characterize CO_2 and brine leakage. In our approach, the workflow of the sensitivity analysis follows Olalotiti-Lawal et al. (2017) whereby three values (low, base, and high) are used for each parameter to address uncertainty. The list and range of parameters included in the sensitivity analysis are summarized in Table 4. Below we discuss details of each parameter that cover the source of the data and a brief theoretical background.

The values and ranges of fracture and matrix permeability related parameters are based on previous simulation studies at this site (Dai et al., 2014; Zhou, 2013). We use constant values for matrix permeability and for the permeability and porosity of the confining layers (caprock and basement). The latter values were the same as those used in a previous simulation study at this site (Stauffer et al., 2013). As described in Section 2.2.2, a step-rate injection and pressure fall-off test is used to calibrate the reservoir model (Onishi et al., 2017). Since the duration of the pump test was short (3 days) and permeability values were modest (~5.9e-14 m^2), pressure propagation was observed only in the vicinity of the injector. As a result, only gridblocks around the injector showed sensitivity with respect to the objective function defined by the sum of differences between observed bottom-hole pressure and simulated bottom-hole pressure at the injector. Although the pump test data was successfully calibrated by adjusting permeability and porosity at gridblocks near the injector, most of the reservoir properties remain uncertain. The sensitive gridblocks used in the calibration were therefore treated as hard data for the sequential Gaussian Simulation (SGS) to generate heterogeneous permeability distributions (Deutsch and Journel, 1998; Remy, 2004). Correlation length, angle and dip are input parameters in SGS used to generate heterogeneous permeability distributions (Remy, 2004). In our application, however, because 1) the storage reservoir is thin, 2) elevation in the reservoir is relatively uniform, and 3) hard data is located at the center, we expect that the flow response obtained from different angle and dip would not be significant. Therefore correlation length was used as a single parameter to represent heterogeneity (Fig. 8).

Matrix porosity is set as a constant value (Zhou, 2013) for simplification, whereas fracture porosity is computed using a correlation with permeability (Bernabé et al., 2003; Deng et al., 2012) to reduce the number of parameters:

$$k = a\phi^b \tag{5}$$

where k is permeability (m^2), ϕ is porosity, a and b are constants depending on different processes and materials. In this study, a = 5.92e-7 and b = 3.0 (Deng et al., 2012). Relative permeability curves used in the sensitivity analysis are presented in Fig. 9. Yoshida et al. (2016) conducted a statistical sensitivity analysis of relative permeability parameters in CO_2 storage and concluded that total CO_2 injected (bottom-hole pressure constraint) is statistically correlated only to the end-point CO_2 relative permeability. Hence, we only use the end-point CO_2 relative permeability as an uncertain parameter for relative

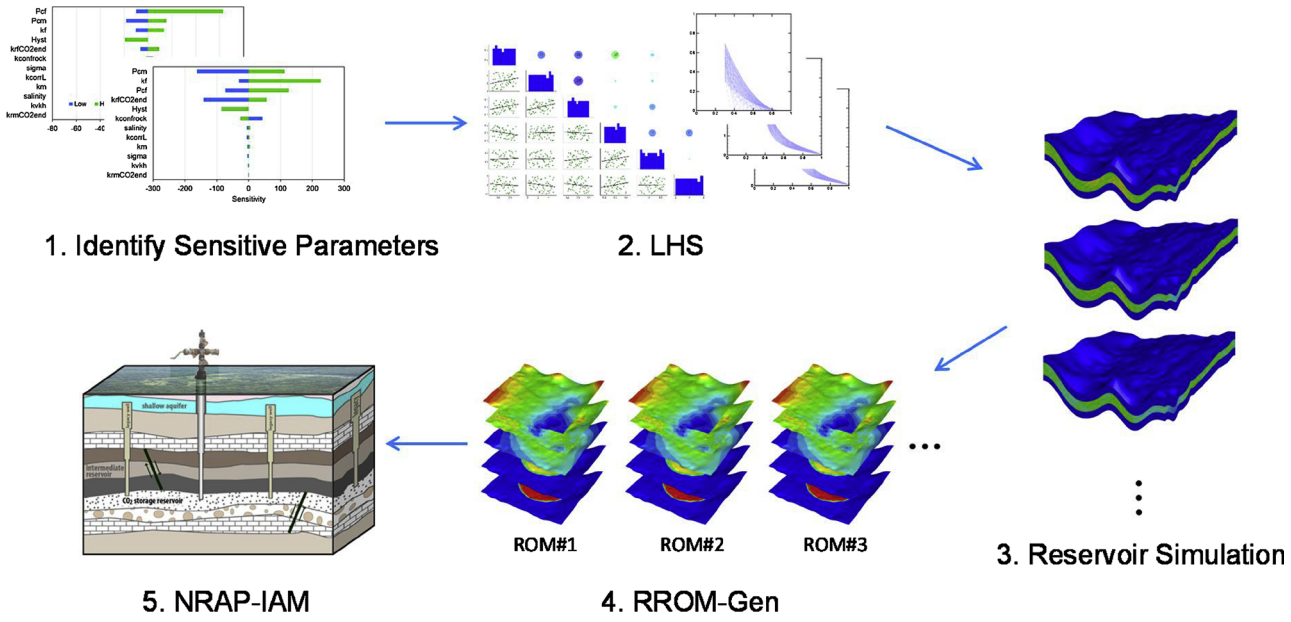

Fig. 7. The risk assessment workflow using the reservoir simulation, RROM-Gen and NRAP-IAM.

permeability functions although the Corey equations have other parameters such as exponents and residual saturation.

Relative permeability hysteresis is an important parameter during GCS (Juanes et al., 2006; Pham et al., 2011) and was therefore included in this study. Different relative permeability curves were used for the drainage and imbibition processes. Several empirical models have been developed to describe hysteresis effects (Carlson, 1981; Killough, 1976; Land, 1968). We used the Land model:

$$S_{CO2,t} = \frac{S_{CO2,i}}{1.0 + CS_{CO2,i}} \tag{6}$$

and,

$$C = \frac{1.0}{S_{CO2,t,\max}} - \frac{1.0}{S_{CO2,\max}} \tag{7}$$

where $S_{CO2,i}$ is the initial CO_2 saturation (CO_2 saturation at flow reversal), C is the Land trapping coefficient, $S_{CO2,max}$ is the maximum CO_2 saturation and $S_{CO2,t,max}$ is the maximum trapped gas saturation. The Killough's method was applied for scanning curves (Killough, 1976). Because the parameters in Eq (7) are not available, the Land trapping coefficient was set at 1.0 (Juanes et al., 2006) for the hysteresis ON case (Table 3).

Capillary pressure plays an important role in CO_2 storage (Alkan et al., 2010; Li et al., 2013; Krevor et al., 2015). During the imbibition process in GCS, small isolated blobs of CO_2 will be trapped by capillary forces which is called capillary trapping or residual trapping (Krevor et al., 2015) and is an important process for maximizing capacity and ensuring the integrity of CO_2 storage. Capillary pressure also controls fracture-matrix interactions in multiple-continuum models (Firoozabadi and Hauge, 1990; Iino and Arihara, 2007). The strength coefficient (P_o) in Eq. (3) is used to explore the sensitivity of capillary pressure curves (Fig. 10). Parameter values and ranges are based on Zhou (2013) and Pruess and Garcia (2002) (Table 2). The same ranges are used for both fracture and matrix capillary pressure curves as a conservative choice and because of parameter uncertainty. Typically, the capillary entry pressure of fractures is smaller than that in the matrix (Wu et al., 2004; Oh et al., 2013); our use of the same values for both fracture and matrix capillary pressure curves is conservative because it may overestimate the CO_2 plume size.

In the dual-porosity dual-permeability model, an additional source/sink term, the transfer function is used to describe fracture-matrix interactions. The transfer function is proportional to a geometrical shape factor σ (m^{-2}), and the driving force is the pressure drop between a matrix grid block and surrounding fractures. A variety of formulations of the transfer function have been proposed (Kazemi et al., 1976; Lim and Aziz, 1995; Warren and Root, 1963). We apply the commonly used approach assuming a pseudo-steady-state flow between fracture and matrix domain suggested by Kazemi et al., 1976:

Table 4
List of possible model sensitivity analysis parameters and their respective assigned bounds.

Parameter	Description	Low	Base	High
kf	Fracture mean permeability (m^2)	3.9e-14	5.9e-14	7.8e-14
kf_Corr	Correlation length for fracture permeability, (m)	1000.0	3000.0	5000.0
kvkh	Vertical fracture permeability anisotropy (-)	0.02	0.50	1.0
k_confrock	Permeability of caprock and basement (m^2)	3.0e-4	3.0e-2	3.0
km	Matrix permeability (uniform), (m^2)	1.0e-14	2.0e-14	3.0e-14
krfCO_2_end	End point CO_2 relative permeability in fracture, (-)	0.30	0.50	0.70
krmCO_2_end	End point CO_2 relative permeability in matrix, (-)	0.10	0.30	0.50
krfCO_2_Hyst	Hysteresis of CO_2 relative permeability in fracture, (-)	ON (C = 1.0) and OFF (base)		
P0f	Strength coefficient of fracture capillary pressure (bar)	0.20	0.30	0.40
P0m	Strength coefficient of matrix capillary pressure (bar)	0.20	0.30	0.40
sigma	Shape factor (m^{-2})	0.12	1.2	5.0
Salinity	Salinity of the aquifer (ppm)	1.0e+4	2.0e+4	3.0e+4

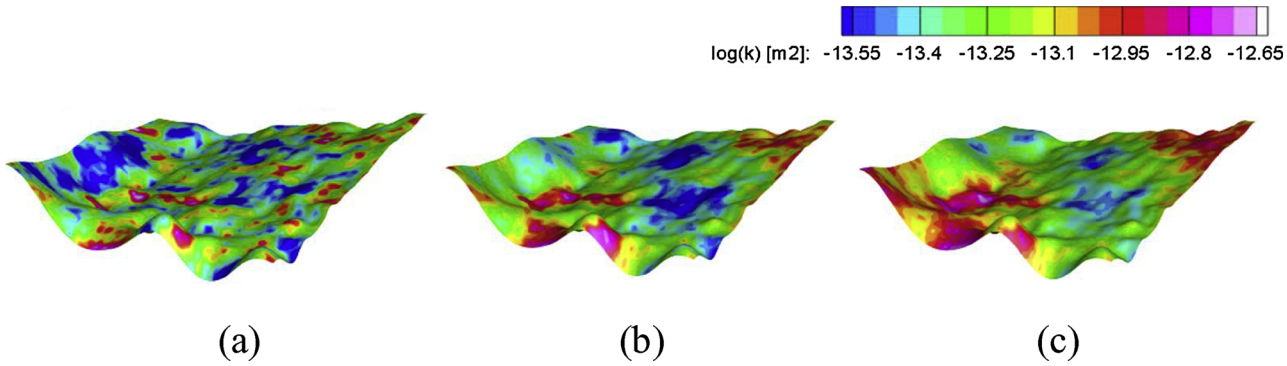

Fig. 8. Heterogeneous permeability fields (top layer of the injection zone). (a) Correlation length = 1000 (m), (b) Correlation length = 3000 (m), and (c) Correlation length = 5000 (m).

$$\sigma = 4.0\left(\frac{1}{l_x^2} + \frac{1}{l_y^2} + \frac{1}{l_z^2}\right) \tag{8}$$

where l_x, l_y, and l_z are the distances (m) between fractures in the x, y, and z directions. Because data for fracture distributions are not available, we apply a constant shape factor (σ) for the entire fracture domain based on (Fakcharoenphol et al., 2014).

Salinity can affect solubility trapping (Barrufet et al., 2010). The salinity range in this study is based on Zhou (2013).

The sensitivity analysis is then carried out using the values and ranges discussed above as follows:

1 Run a single reservoir simulation with the base values shown in Table 4
2 Use RROM-Gen and generate lookup table inputs for the NRAP-IAM
3 Run the NRAP-IAM using fixed settings (Table 3) to conduct fair comparisons of parameter sensitivity
4 Save a realization (50 percentile) from each leakage rate obtained from the NRAP-IAM (step 3)
5 Select 1 parameter in Table 4 and perturb (i.e., low or high) and run a reservoir simulation using the updated value. Then, go to the step 2.

The NRAP-IAM calculations are conducted with parameters given in Table 3 except for the wellbore cement quality which is held constant to conduct comparisons of the impact of reservoir parameters on injection. Step 2 through step 5 are repeated until all parameters in Table 4 are covered, requiring 24 runs (1 base + 11 × 2 low and high for parameters except hysteresis + 1 with hysteresis). The graphical description of the workflow is presented in Fig. 11.

The relative sensitivity of the m^{th} parameter obtained from the sensitivity study is computed using the dimensionless scaled sensitivities (Hill, 2000; Olalotiti-Lawal et al., 2017) which is the ratio of the change in the objective function, $O(m)$ to the relative perturbation in the parameter. The dimensionless sensitivity, defined in the following equation, eliminates disproportionate parameter perturbation sizes and dimensions:

$$Sensitivity_m = \frac{O(m)}{\Delta x_m} x_m^{Base} \tag{9}$$

where x_m is a value of parameter m, and the objective function is defined as L2 norm of the difference of the computed leakage when the m^{th} parameter is used relative to the computed leakage from the base case over the entire simulated time, scaled by the standard deviation of the base case:

$$O(m) = \sum_{k=1}^{Ntstep} \frac{||g_k(m) - d_{Base,k}||_2}{\sigma_m} \tag{10}$$

where *Ntstep* is the number of time steps, g_k (m) is a cumulative leakage at time step k when the m^{th} parameter is used, $d_{Base,k}$ is a cumulative leakage of the base case at time step k, and σ_m is the standard deviation of the cumulative leakage of the case m. σ_m is used to scale the objective function for comparison purposes between different metrics including CO_2 and brine leakage to the atmosphere and the shallowformations.

4.1.2. Results

The results of the dimensionless scaled sensitivity studies using Eqs. (9) and (10) are summarized in tornado diagrams (Figs. 13 and 14) and are based on computed leakage using NRAP-IAM (Fig. 12). We found that fracture permeability, capillary pressure in fracture and matrix, fracture end-point CO_2 relative permeability, permeability of the confining rocks, and hysteresis effects were key parameters. Visual comparisons of the CO_2 plume between the base case and cases with low and high values of key parameters are provided in Fig. 15 in which we see results consistent with the sensitivity analysis. The dominance of fracture permeability is clear (Fig. 15 **(a)-(c)**) as a primary control on

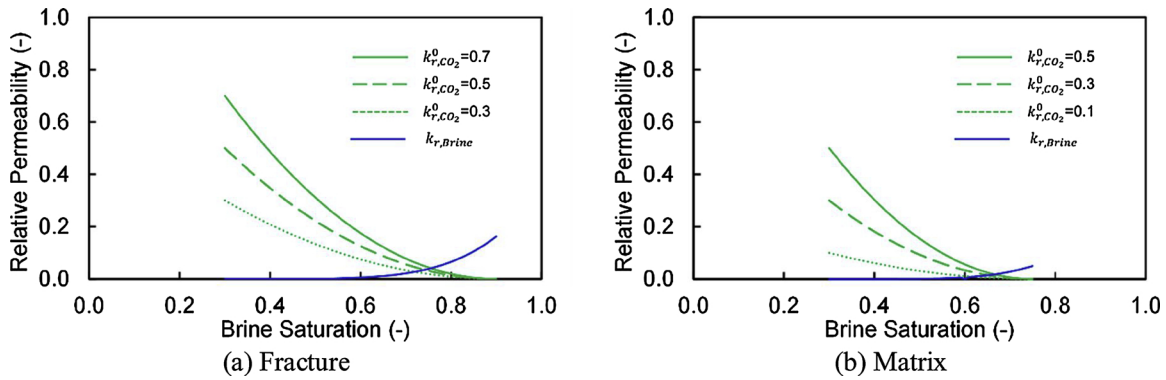

Fig. 9. Relative permeability curves.

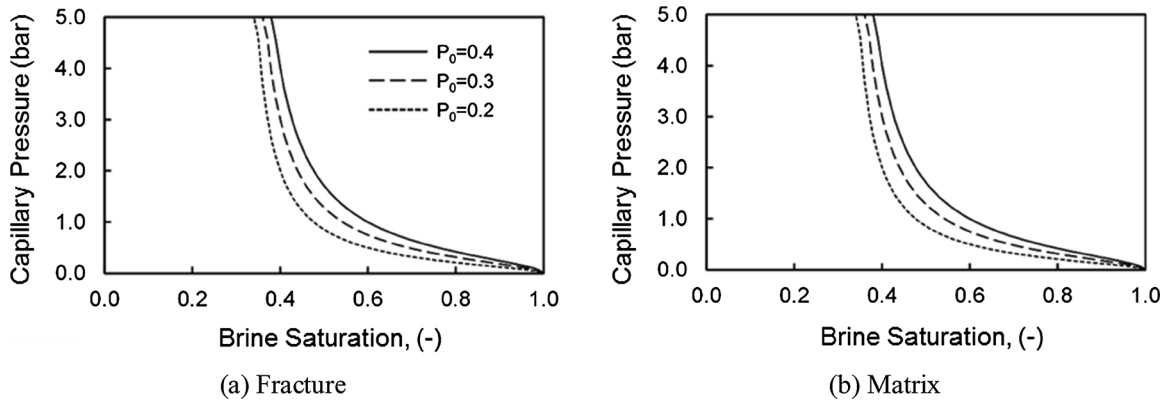

Fig. 10. Capillary pressure curves for the fracture and matrix domains.

plume geometry. The other key parameters are capillary pressure for fracture and matrix. When fracture capillary pressure is higher than matrix capillary pressure, more CO_2 migrates into the matrix domain, and vice versa (Fig. 15 **(d)-(i)**), consistent with the DPDP formulation (Blaskovich, et al., 1983; Iino and Arihara, 2007; and others). Leakage is sensitive to fracture end-point CO_2 relative permeability (Fig. 15 (j)-**(l)**) as suggested by Yoshida et al. (2016). Likewise, leakage is sensitive to the permeability of the confining rocks (Fig. 15 **(m)-(o)**) which confirms results from Dai et al., (2014). Last, hysteresis shows negative correlation with CO_2 and brine leakage (Fig. 15 **(p)-(q)**) as suggested by Juanes et al. (2006) and Pham et al. (2011). It is informative to mention that results obtained from the previous simulation study at this site by Dai et al. (2014) and other studies of GCS (Pawar et al., 2016; Deng et al., 2012) concluded that the heterogeneity of permeability distribution is one of the key parameters in GCS, whereas we find that permeability heterogeneity is relatively less important. One possible reason is that the range of permeability values used here is based on Zho et al. (2013) and is much narrower than what Dai et al. (2014) used and thus permeability heterogeneity shows little influence in our study as illustrated in Fig. 16 **(a)-(c)**. Another reason could be the values of correlation length used in this study. These lengths are relatively large in comparison with the domain size such that the domain can be locally

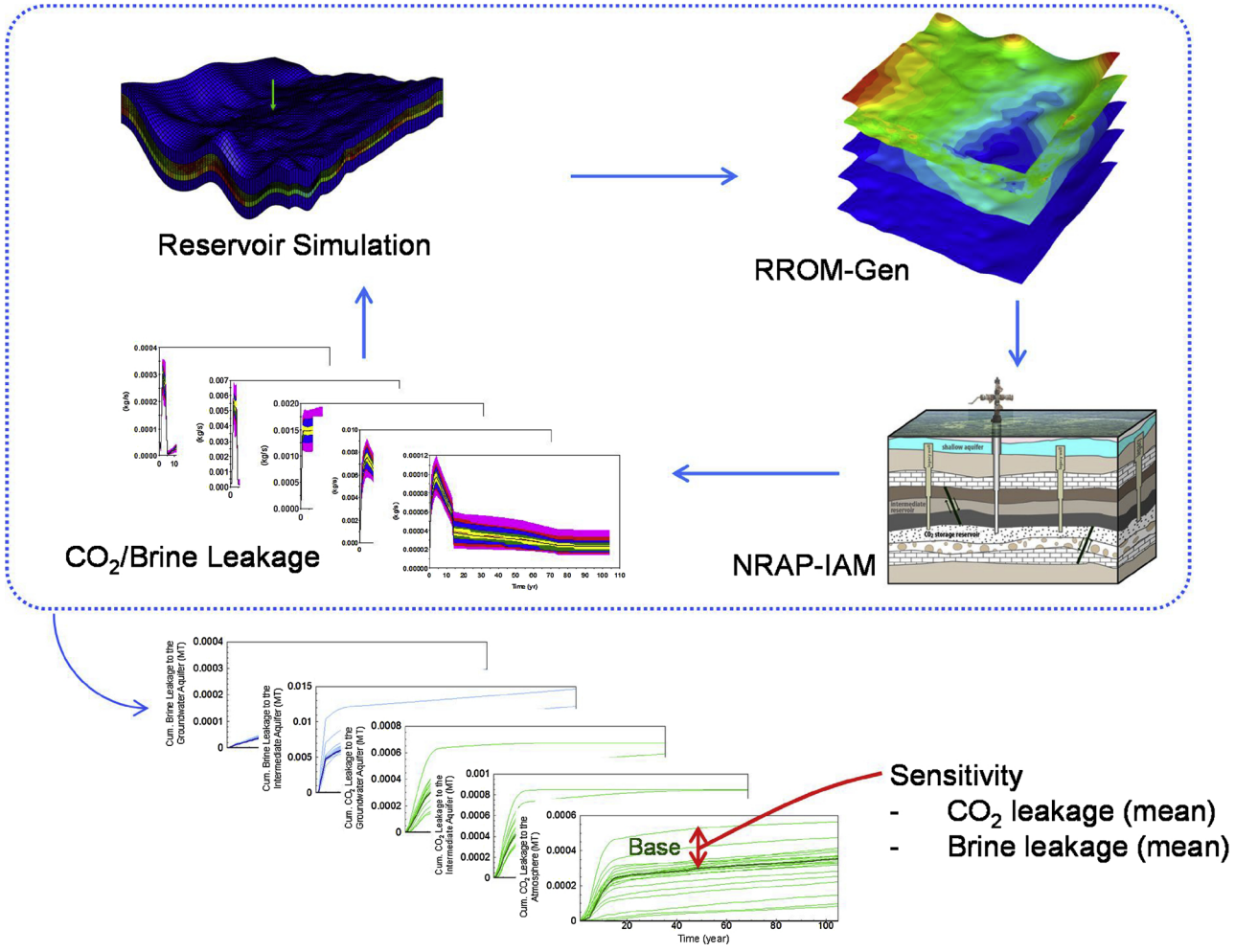

Fig. 11. The sensitivity analysis workflow.

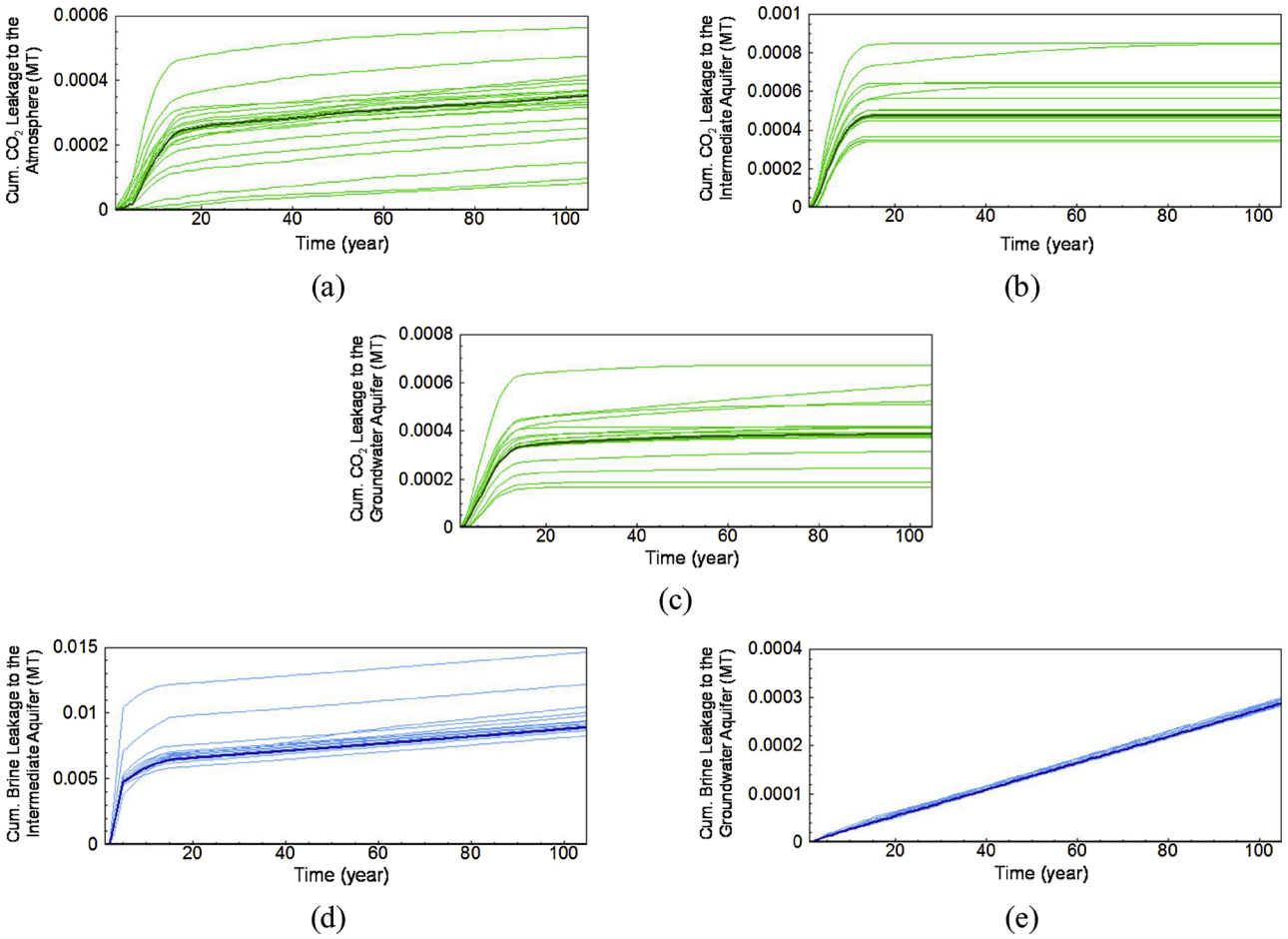

Fig. 12. Sensitivity analysis results: (a) CO_2 leakage to the atmosphere, (b) CO_2 leakage to the intermediate aquifers, (c) CO_2 leakage to the groundwater aquifer, (d) Brine leakage to the intermediate aquifers, (e) Brine leakage to the groundwater aquifer (green line is the base case) (For interpretation of the references to colour in this figure legend, the reader is referred to the web version of this article).

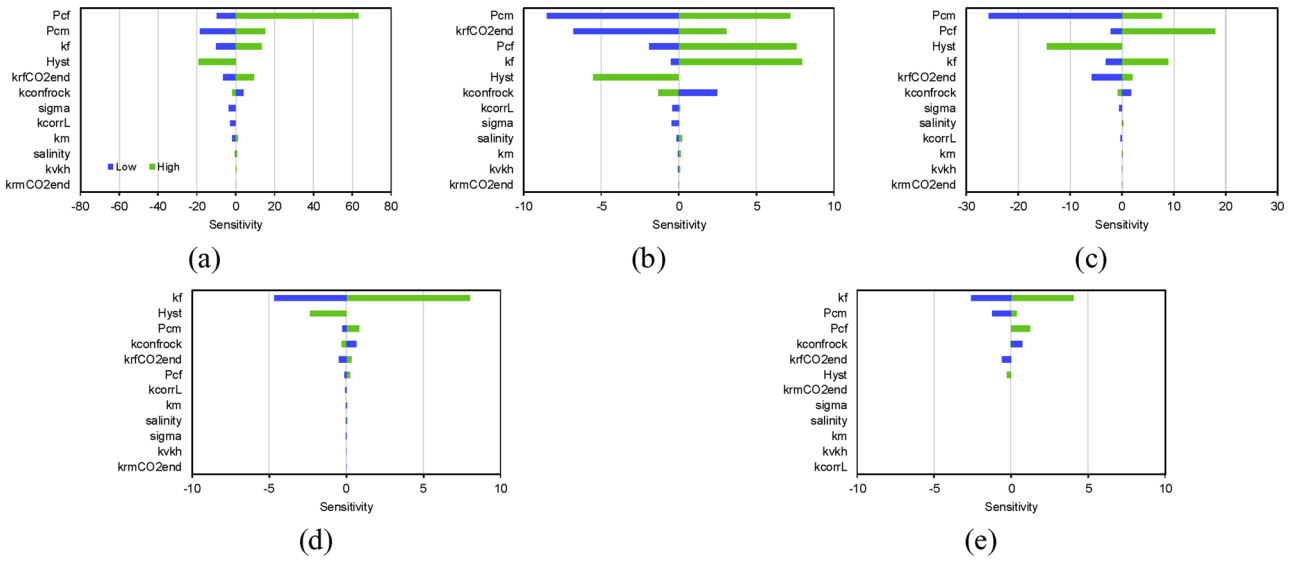

Fig. 13. Tornado chart of the dimensionless scaled sensitivity of model parameters for the injection period (4 years): (a) CO_2 leakage to the atmosphere, (b) CO_2 leakage to the intermediate aquifers, (c) CO_2 leakage to the groundwater aquifer, (d) Brine leakage to the intermediate aquifers, (e) Brine leakage to the groundwater aquifer.

homogeneous, resulting in little influence of permeability heterogeneity. Similar conclusions can be made for vertical permeability anisotropy (kv/kh). Dai et al. (2014) and other studies of GCS in saline aquifers (Chanbari et al. 2006; Kumar et al. 2004) showed that the magnitude of kv/kh significantly affects GCS in saline aquifers, but again, the narrower range for kv/kh used in this study compared to

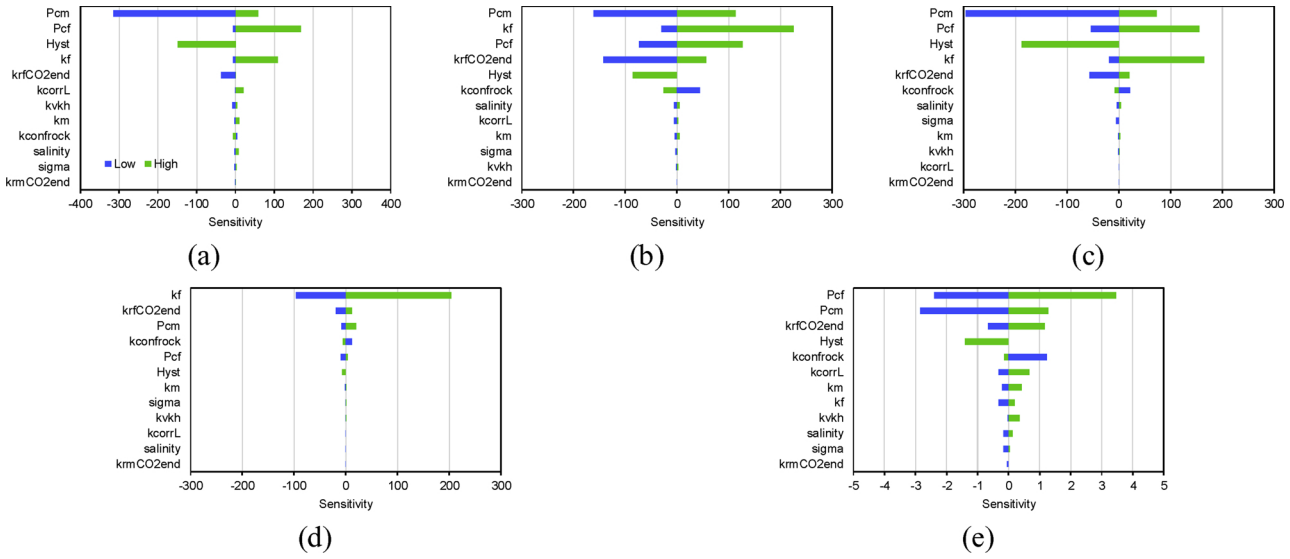

Fig. 14. Tornado chart of the dimensionless scaled sensitivity of model parameters for the post-injection period (100 years): (a) CO_2 leakage to the atmosphere, (b) CO_2 leakage to the intermediate aquifers, (c) CO_2 leakage to the groundwater aquifer, (d) Brine leakage to the intermediate aquifers, (e) Brine leakage to the groundwater aquifer.

others results in limited influence (Fig. 16**(d)-(f)**). The relatively uniform elevation of the injection zone may be another reason why kv/kh is found to be less important in this study. In fact, there is an up dip at the edge of the injection zone, however, there is little chance for the CO_2 plume to reach the region as observed in Fig. 15. Fig. 17 visually illustrates the effects of caprock permeability on the shape of the simulated CO_2 plumes.

Through this exercise, we find that the potential amount of CO_2 leakage is most sensitive to values of 1) injection horizon permeability, 2 + 3) capillary pressure in both the fracture and matrix, 4) fracture end-point CO_2 relative permeability, 5) hysteresis of the fracture CO_2 relative permeability, and 6) the permeability of the confining rocks. These parameters are then used as representative uncertain parameters for the storage reservoir component in the NRAP-IAM (Fig. 1). Note that this conclusion could be different depending on the locations and quality of legacy wells. It should also be noted that solely using tornado diagrams to screen out parameters might not be a best practice in nonlinear cases where interactions between parameters can be significant. For such cases, it is recommended to use a more sophisticated approach (e.g., Bhark and Dehghani, 2014). In our application, however, this simple approach can provide intuitive understanding of uncertain parameters and, thus, is sufficient to demonstrate the uncertainty quantification workflow using the NRAP-tools.

4.2. Reservoir simulation

4.2.1. Methods

We applied LHS to reduce the number of realizations and efficiently conduct our analysis. Fewer numerical simulations are required to cover the same range of uncertainties in the developed workflow compared to previous approaches in which 3^N simulations, where N is the number of uncertain parameters, are required. Following the above recommendations, we select 6 sensitive parameters from the sensitivity analysis. Therefore, $3^6 = 729$ numerical reservoir simulations are required if the previously suggested (Jordan et al., 2015) approach is used. Because reservoir simulation runs can take days depending on the combination of the parameters, the previous approach is not suitable when available information of the storage reservoir is limited, which is rather common in GCS in saline aquifers. In contrast, for this study, we apply LHS and sample 50 realizations for reservoir simulation using the 6 sensitive parameters obtained from the sensitivity analysis. We select 50 realizations because this entire workflow is intended for a wide range of users including research institutes, universities, and industry. For those who do not have sufficient computational facilities to conduct hundreds or thousands of full 3-D reservoir simulations, the new approach utilizing LHS method will prove more accessible. More importantly, the quality of the legacy well cements specified in the NRAP-IAM have a larger impact on leakage results than the variability seen in the LHS reservoir simulations. This will be further discussed in the Section 4.3.2.

One of the 6 chosen sensitive parameters is hysteresis of fracture CO_2 relative permeability, for which a constant value of the Land trapping coefficient was used in the sensitivity study ($C = 1.0$). Here we provided a range for Land trapping coefficient between the values $0.2 < C < 5.0$ (Krevor et al., 2015). The significance of C is illustrated in Fig. 18. Higher C results in less trapping (i.e., similar drainage and imbibition curves), and vice versa.

4.2.2. Results

Based on the sensitivity analysis presented in the previous section, LHS is performed for the 6 most sensitive parameters and the results are summarized in Fig. 19 in which scatter plots show correlations between parameters (bottom-left), whereas values on top-right are corresponding correlation coefficients and size of makers are proportional to correlation coefficients. As seen in the Fig. 19, none of parameters are strongly correlated, meaning that parameters are efficiently sampled, or sampled realizations cover a wide range of uncertainties.

The ensemble of simulation results of cumulative CO_2 injected during the first six years are overlaid in Fig. 20 with P10, P50, and P90 (percentile) probability values based on total amount of CO_2 injected at the end of injection period. Realizations with high permeability, high Land trapping coefficient, and high strength coefficients for fracture and matrix capillary pressure yield higher total injected CO_2 (Fig. 20). One interesting factor here is that fracture CO_2 end-point relative permeability in P10 is higher than that of P50 and P90. This is because the injectivity is strongly affected by permeability values at completion gridblocks although end-point relative permeability is an important parameter determining the size and shape of the CO_2 plume as discussed in the sensitivity analysis section. We also obtain results that differ from the conclusion of the previous simulation study at this site by Dai et al. (2014). The previous work found a four year maximum injected mass of approximately 5.0 MT of CO_2 with the same well

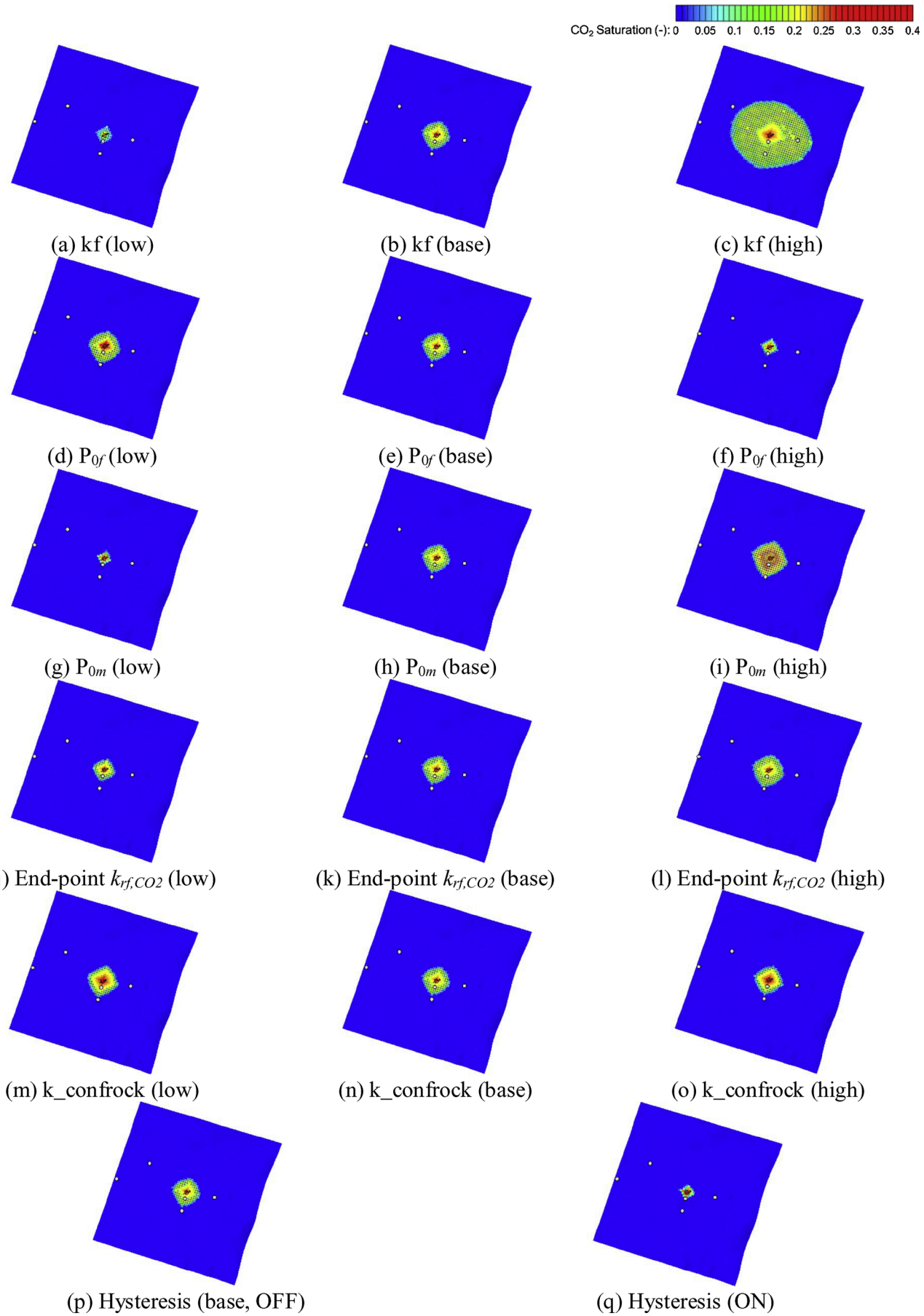

Fig. 15. CO_2 saturation profiles in the reservoir for sensitive parameters at the end of injection period.

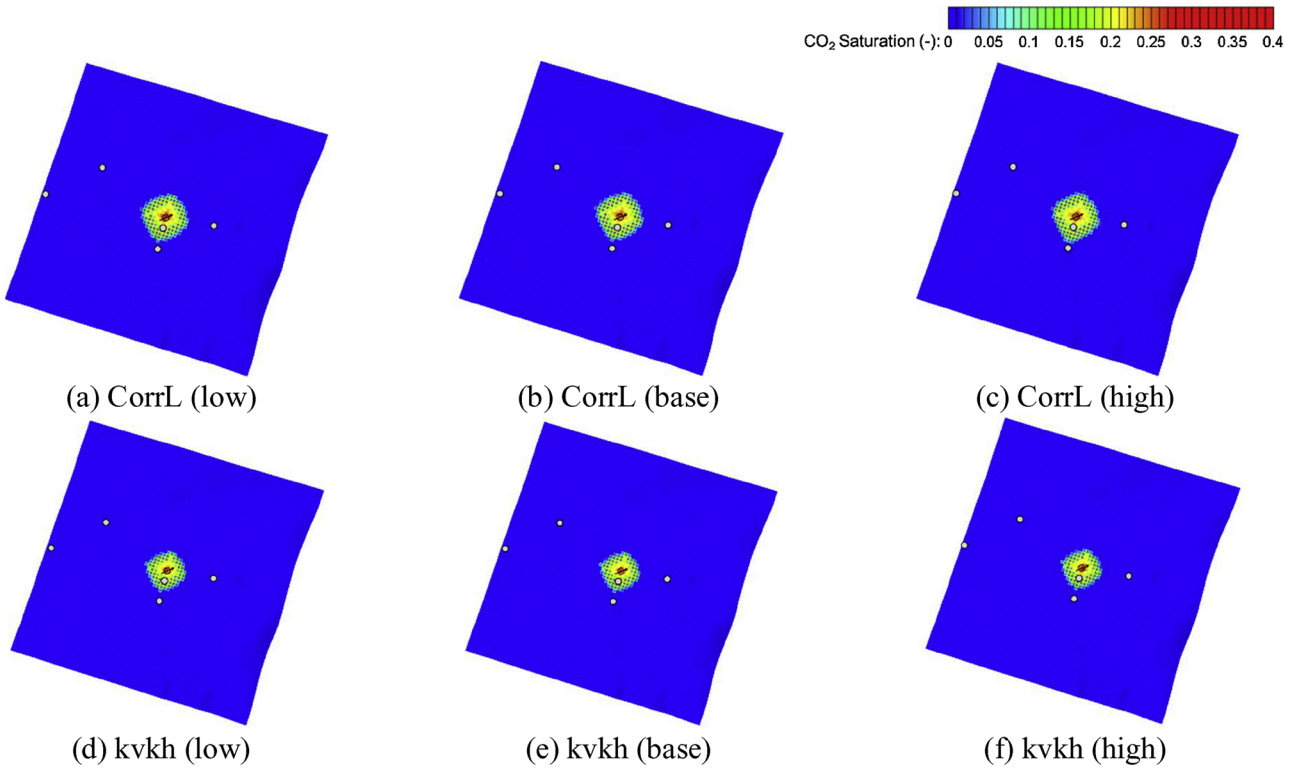

Fig. 16. Further investigation of parameters used in the sensitivity analysis: insensitive parameters including correlation length and kvkh at the end of injection period.

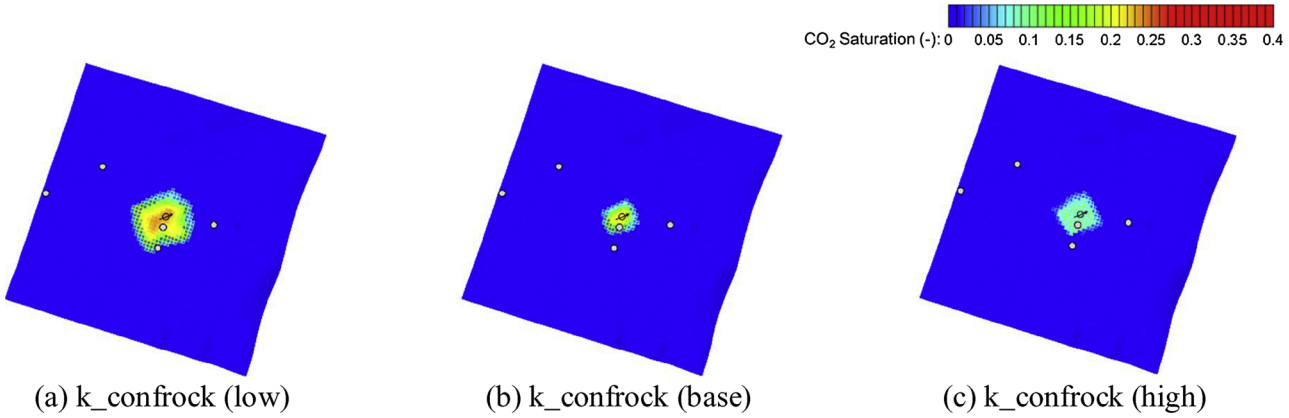

Fig. 17. CO_2 saturation profiles of low, base, and high confining rock permeability cases at the end of monitoring (104 years).

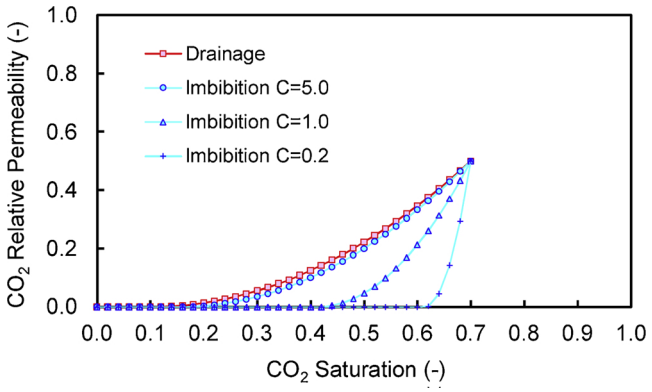

Fig. 18. CO_2-Brine relative permeability functions, an illustration of hysteresis.

constraint, whereas our results predict that the maximum mass of CO_2 that can be injected in four years is around 1.2 MT. Based on Fig. 20, our study finds a low (4.0%) likelihood of successfully injecting 1.0 MT/yr (target injection rate) into the storage reservoir as compared to 58% probability of successful injection of 1 MT/yr reported by Dai et al. (2014). One possible reason is that ranges for static data such as permeability of the injection zone and the confining rocks used by Dai et al., (2014) are much wider that what we are using here. More importantly, the effect of hysteresis was included in our study which can significantly affect trapping mechanisms and thus the size of the CO_2 plume as depicted in Fig. 15. Our results show more trapping with hysteresis effects and therefore BHP at the injector more easily reaches 18.5 MPa (hydro-fracture limit) resulting in a reduced amount of CO_2 injected.

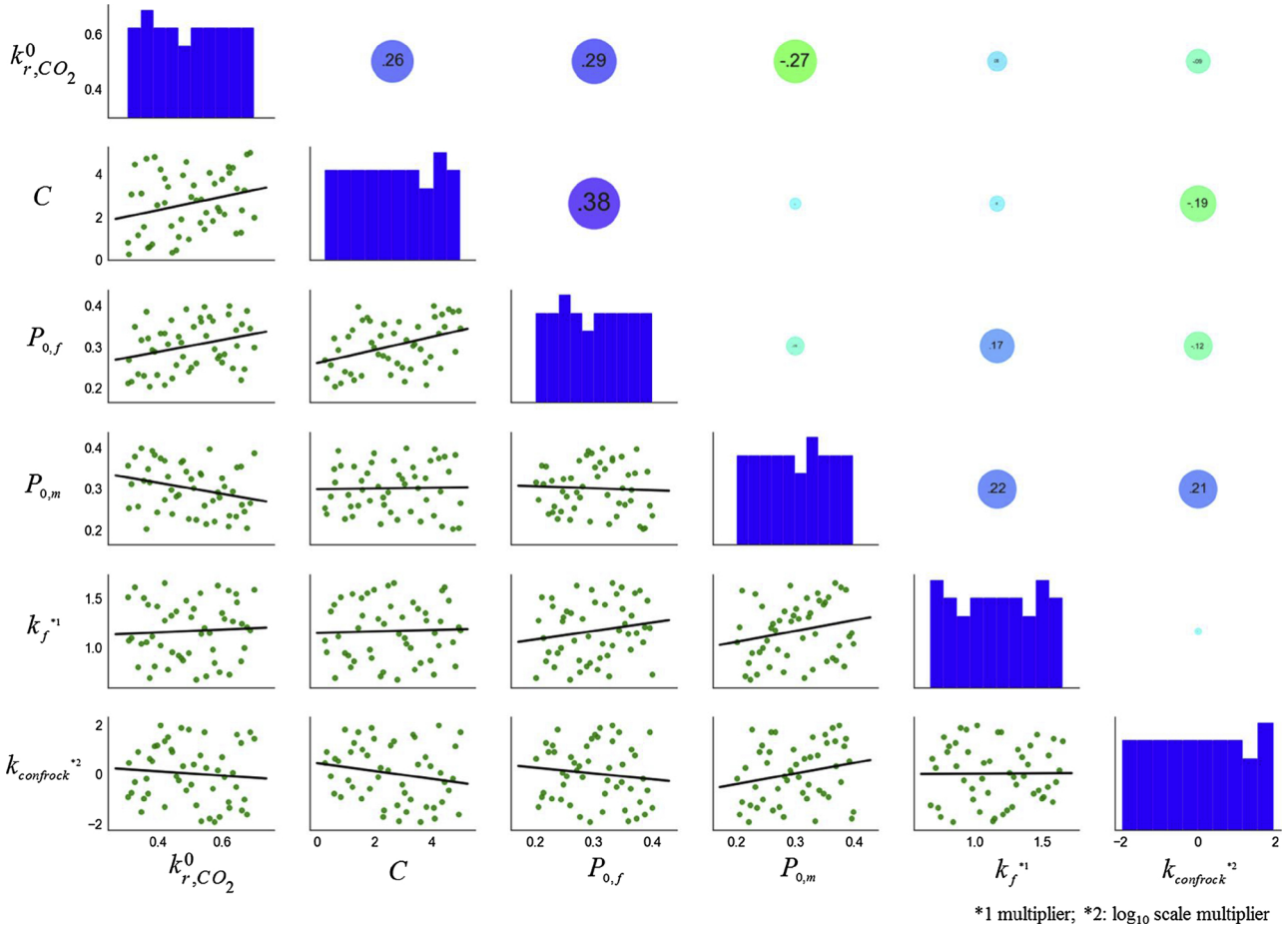

Fig. 19. Correlation matrix for 6 parameters generated from LHS.

4.3. NRAP-IAM simulation

The application of the NRAP-IAM is demonstrated in this section. We first present simulation results of the NRAP-IAM with the base case scenario, followed by analysis of wellbore integrity using Monte-Carlo sampling.

4.3.1. CO_2 and brine leakage calculation for the base case

The NRAP-IAM simulation results use 50 lookup table ROMs, extracted from 50 full 3-D reservoir simulations using RROM-GEN, which represent time dependent pressure, temperature, supercritical CO_2 mass fraction, and dissolved CO_2 at the top of the storage formation (Fig. 5). The lookup tables are combined with other input data for shallow formations and legacy wells (Table 3). Calculated leakage is summarized in Fig. 21 showing cumulative CO_2 and brine leakage to the shallow formations. CO_2 leakage to the atmosphere is predicted to be negligible and thus not shown here. While we see P10, P50, and P90 (percentiles) in brine leakage to the shallow formations (thick lines in Fig. 21**(c) and (d)**), only P90 can be seen in CO_2 leakage to the shallow formations (thick lines in Fig. 21**(a) and (b)**). This is because more than half of realizations predict no leakage due to low wellbore permeability or combination of sampled paremeters resulting in low leakage (e.g., low fracture permeability, low CO_2 end-point relative permeability, etc.).

4.3.2. Wellbore integrity

Wellbore integrity is an important parameter in GCS (Carey, 2013; Carey et al., 2009, 2010; Crow et al., 2010). A built-in log normal probability distribution (Table 3) for wellbore cement quality is used for the base case presented in the previous section, because wellbore integrity information is not available for all legacy wells; however wider ranges of cement quality are used in the Big Sky NRAP-IAM simulations to investigate the impact of wellbore integrity at this site. In our application, we test 5 scenarios in which we use a single constant permeability (cement quality) value for all wells in each case. Recent global analysis indicates that maximum acceptable leakage rates are between 0.01 percent and 1.0 percent leakage per year (Kutz and Elkamel, 2010). The following equation is applied to calculate the CO_2 leakage rate to the atmosphere:

$$CO_2\ Leakage\ (\%/year) = 100.0 \times \frac{CO_2\ Leakage\ Rates\ (MT/year)}{Cumulative\ CO_2\ Injected\ (MT)} \quad (11)$$

Simulation results over first 50 years are summarized in Fig. 22 in which 50 realizations are sampled for each scenario (different wellbore integrity values) and the green shade is acceptable CO_2 leakage (0.01 percent) range. The ensembles with different colors correspond to different wellbore cement qualities and each set of the ensemble with the same color contains 50 realizations. Variation of CO_2 leakage rates within the same color essentially arises from varying RROMs. Fig. 22 shows that unless cement permeability quality is extremely poor (i.e., larger than 10 Darcy (9.87e-12 m^2)), GCS in the Kevin Dome is expected to be secure over the entire monitoring period according to the selected criteria. Some realizations (realization #3, 29, 36) show unacceptable leakage rates even after the injection period (red circle). Parameters of these realizations are revisited as depicted in the bottom part of Fig. 22 to determine what is causing this behavior. We confirm that for these leaks, higher fracture permeability, lower confining rock permeability, and higher Land's trapping coefficient result in higher CO_2 leakage rates that are also strongly affected by the combination of the capillary pressure in both fracture and matrix as observed in Sections 4.1 and 4.2.

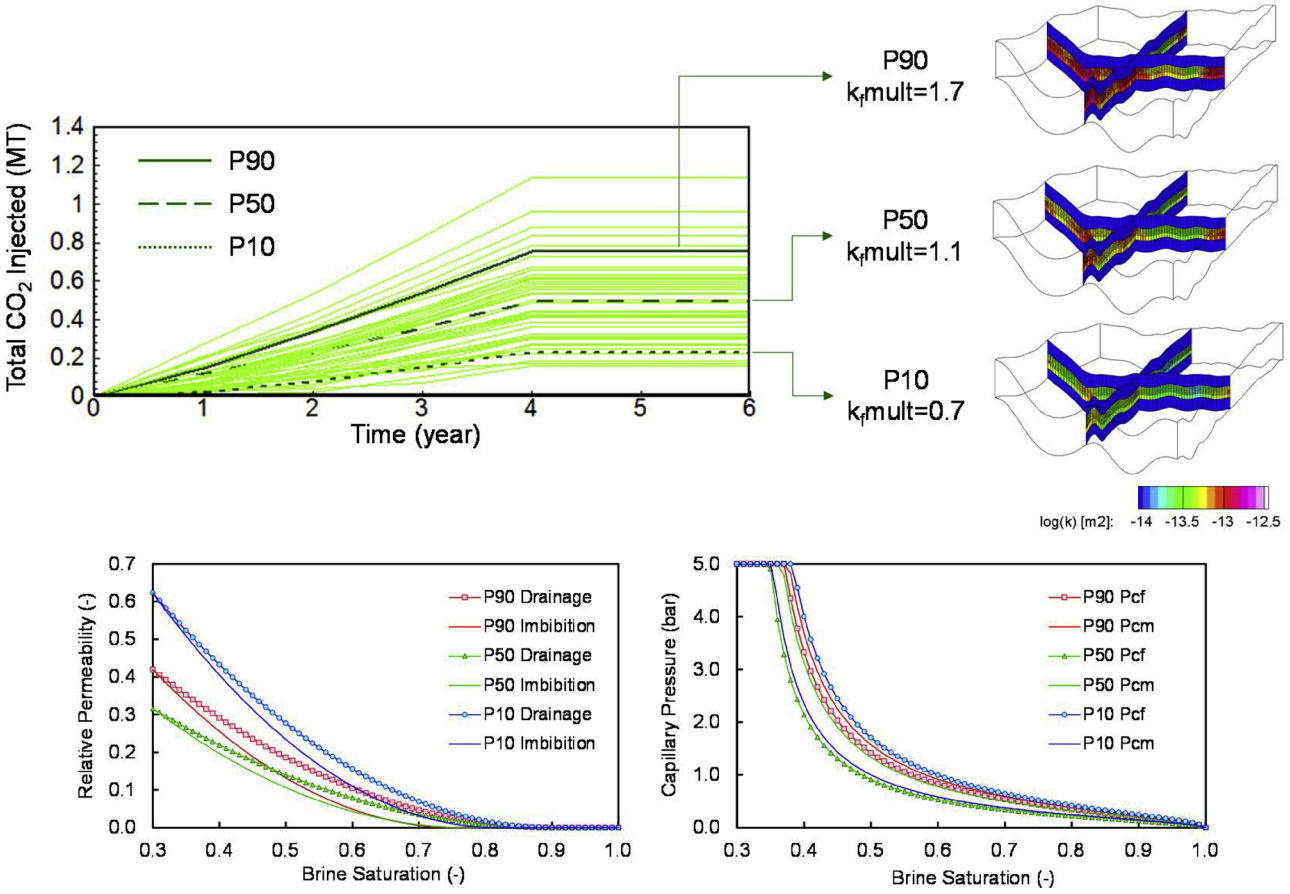

Fig. 20. Reservoir simulation results: total amount of CO_2 injected with P10, P50 and P90 probability ranges.

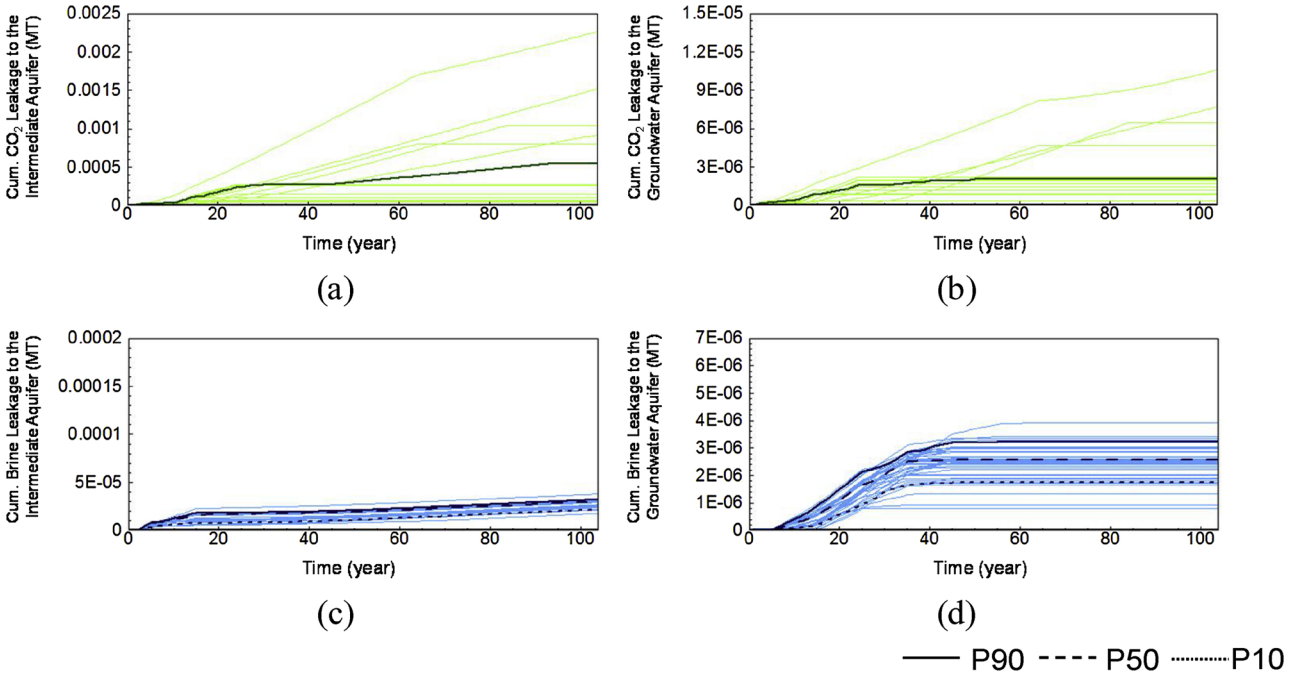

Fig. 21. NRAP-IAM base case results: (a) CO_2 leakage to the intermediate aquifers, (b) CO_2 leakage to the groundwater aquifers, (c) Brine leakage to the intermediate aquifers, and (d) Brine leakage to the groundwater aquifers. Thick lines are percentiles: P90 (solid line), P50(dash line), and P10 (dot).

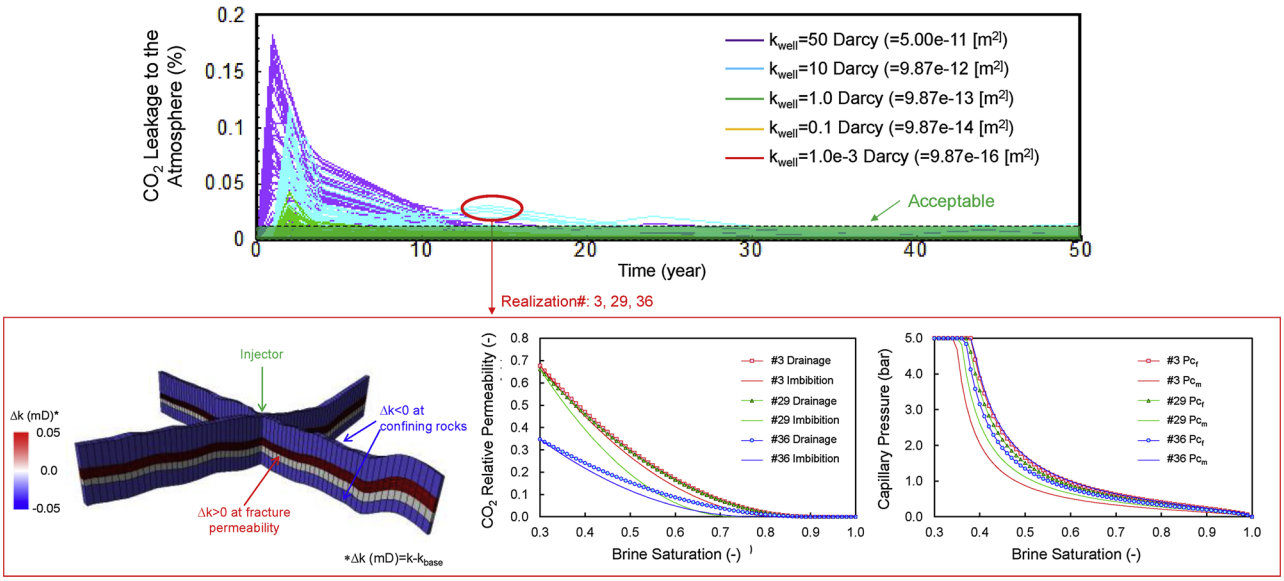

Fig. 22. NRAP-IAM simulation results of wellbore cement quality sensitivity (top) and parameters of realizations (realization#3, 29, 36) that showed unacceptable leakage rates.

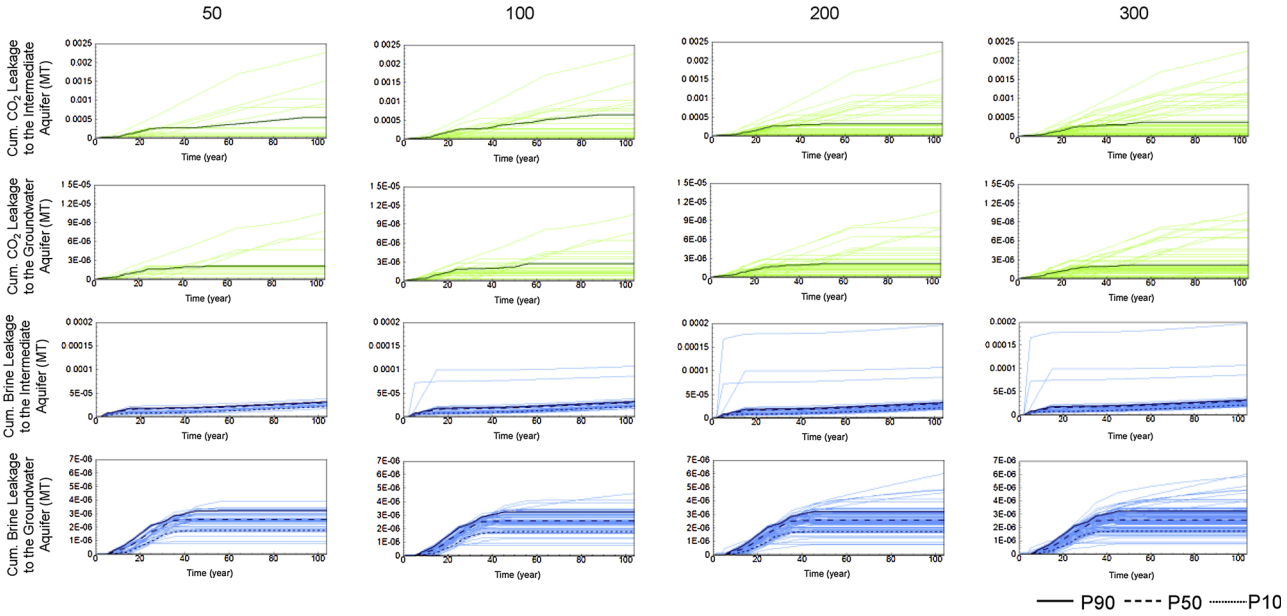

Fig. 23. Convergence analysis results for Monte Carlo sampling in NRAP-IAM with columns giving the number of samples. Results for CO_2 and brine in the intermediate aquifer and groundwater are shown.

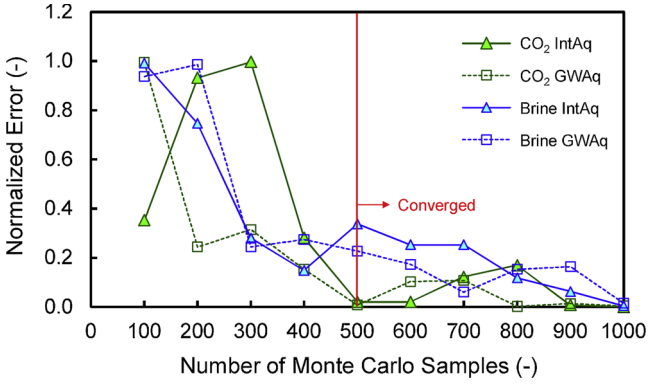

Fig. 24. Convergence analysis results for Monte Carlo sampling in NRAP-IAM.

Nevertheless, leakage rates in all cases converge within the acceptable leakage rates after 30 years. This observation is useful to determine, for example, duration of monitoring of this site.

4.3.3. *Convergence analysis of the NRAP-IAM*

The NRAP-IAM gives slightly different results in every simulation when risk assessment is performed using 50 realizations. It is worthwhile to study the impact of the number of realizations for Monte-Carlo sampling in the NRAP-IAM to determine the optimum number of samples for convergence. We again used the data from Table 3 for shallow formations and wellbores and 50 sets of ROMs for the storage reservoir. While constant values are used for thickness, permeability, and porosity for the shallow aquifers, a built-in log normal distribution is used for wellbore cement quality uncertainties. Starting from 50 realizations, the number of realizations was increased up to 1000 with increments of 100 (50 in the first step). Selected results are presented in

Fig. 23. CO_2 leakage to the atmosphere is predicted to be negligible and thus not shown here. A more quantitative analysis was conducted comparing the L2 norm of difference of P10, P50, P90 values (probability percentiles) using the following equation:

$$Error_j = \sum_{i=1}^{Nstep} [||P10_{i,j}^{n} - P10_{i,j}^{n-1}||_2 + ||P50_{i,j}^{n} - P50_{i,j}^{n-1}||_2 + ||P90_{i,j}^{n} - P90_{i,j}^{n-1}||_2] \quad (12)$$

where n represents the number of samples (e.g., n: number of samples = 200 and n-1:number of samples = 100), thus, $P10_{i,j}^{n}$ represents P10 of n^{th} step and j^{th} leakage metrics at i^{th} time step, and same for other percentiles. Note that the calculated errors are normalized in such a way that the maximum and minimum values become 1.0 and 0.0, respectively.

Fig. 24 plots results obtained from this analysis, from which all leakage rates show steep reductions of error after 400 realizations. The optimum number of realizations for this specific example is therefore between 500 and 600. Small errors are seen beyond 500 realizations, however, these are because of the nature of Monte-Carlo random sampling: the NRAP-IAM shows slightly different results in every run, which is inevitable. Unfortunately, the optimum number of realizations in the NRAP-IAM is case dependent and therefore investigation of the optimum number of realizations and engineering judgements are necessary in each specific case. One interesting factor here is that error starts low for CO_2 leakage to the intermediate aquifer then increases unlike other metrics. This is because P90 values in the 50 and 100 realization cases for CO_2 leakage to the intermediate aquifer are similar, whereas these converge to slightly lower values when the number of realizations is ≥ 200 (1st row in Fig. 23). As a result, the error becomes larger at 200 realizations, and then decreases beyond 300 realizations. The other important factor here is that rapid analytical calculations (usually order of minutes) and the powerful stochastic framework of the NRAP-IAM allows users to explore a variety of analyses, even for field-scale applications, within realistic simulation times that would be difficult to achieve solely with full physics, 3-D numerical simulations or analytical methods. It is informative to mention that convergence analysis of Monte-Carlo sampling is typically done by comparing sample variance at different number of samples. It is known that convergence behavior of Monte-Carlo sampling typically follows log scale (Ballio and Guadagnini, 2004). This means that increasing the number of Monte-Carlo samples from 100 to 200 to obtain a better stabilization of the results has basically no effect on convergence of Monte-Carlo sampling. In other words, it is necessary to use an order of magnitude greater number of samples to see significant effects. In our application, however, the use of thousands of samples can be computationally expensive in terms of both processors and memory and may not be practical, even with the rapid simulation ability of the NRAP-IAM. Instead, as we are interested in convergence of calculated leakage rather than convergence of Monte-Carlo sampling itself, we recommend the use of Eq. (12) as an objective function to quantify convergence of the NRAP-IAM simulations.

5. Summary and Conclusion

1 NRAP tools have been successfully applied to risk assessment of GCS for a fractured saline aquifer, Kevin Dome in Montana.
2 The maximum total mass of CO_2 injected into the middle Duperow is predicted to be 1.2 MT. This is lower than the estimate by Dai et al., (2014) because of different parameter settings, such as ranges for permeability and the inclusion of hysteresis effects in the current study.
3 The newly developed workflow for the NRAP-IAM (using LHS to generate realizations for full 3-D numerical simulations) can significantly reduce computational requirements compared to the previously suggested workflow. The powerful stochastic framework is capable of risk assessment in field-scale applications.
4 The potential amount of CO_2 and brine leakage is most sensitive to values of fracture permeability, capillary pressure in both the fracture and matrix, end-point fracture CO_2 relative permeability, permeability of confining rocks, and hysteresis in the CO_2 relative permeability.
5 GCS in the Kevin Dome has little risk of CO_2 leakage to the atmosphere unless the quality of the legacy wells is extremely poor.

Future work will incorporate more detailed injection reservoir characterization including lithofacies classification, seismically conditioned reservoir property modeling, distribution of fracture networks and their impact on permeability heterogeneity. The inclusion of these conditioning data and methods will affect predicted pressure and CO_2 saturation distributions over the extent of injection. The addition of fracture networks, as preferential flow paths, is expected to have a significant influence on CO_2 plume dynamics and the leakage rate upward to multiple susceptible USDW aquifers. Additionally, potential CO_2 and brine leakage through fault pathways is also under consideration using the NRAP fault ROM (Nguyen et al., 2017a).

Disclaimer

This report was prepared as an account of work sponsored by an agency of the United States Government. Neither the United States Government nor any agency thereof, nor any of their employees, makes any warranty, express or implied, or assumes any legal liability or responsibility for the accuracy, completeness, or usefulness of any information, apparatus, product, or process disclosed, or represents that its use would not infringe privately owned rights. Reference herein to any specific commercial product, process, or service by trade name, trademark, manufacturer, or otherwise does not necessarily constitute or imply its endorsement, recommendation, or favoring by the United States Government or any agency thereof. The views and opinions of authors expressed herein do not necessarily state or reflect those of the United States Government or any agency thereof.

Acknowledgements

This material is based upon work supported by the U. S. Department of Energy and the National Energy Technology Laboratory under Award Number DE-FC26-05NT42587.

References

Alkan, H., Cinar, Y., Ülker, E., 2010. Impact of capillary pressure, salinity and in situ conditions on CO_2 injection into saline aquifers. Transp. Porous Media 84, 799–819.
Bachu, S., 2000. Sequestration of CO_2 in geological media: criteria and approach for site selection in response to climate change. Energy Convers. Manage. 41, 953–970.
Ballio, F., Guadagnini, A., 2004. Convergence assessment of numerical Monte Carlo simulations in groundwater hydrology. Water Resour. Res.
Bao, J., Hou, Z., Fang, Y., Ren, H., Lin, G., 2013. Uncertainty quantification for evaluating impacts of caprock and reservoir properties on pressure buildup and ground surface displacement during geological CO_2 sequestration. Greenh. Gases Sci. Technol. 3, 338–358.
Barrufet, M.A., Bacquet, A., Falcone, G., 2010. Analysis of the storage capacity for CO_2 sequestration of a depleted gas condensate reservoir and a saline aquifer. J. Can. Pet. Technol. 49, 23–31.
Bernabé, Y., Mok, U., Evans, B., 2003. Permeability-porosity relationships in rocks subjected to various evolution processes. Pure Appl. Geophys. 160, 937–960.
Bhark, E.W., Dehghani, K., 2014. Assisted history matching benchmarking: design of experiments-based techniques. SPE Annual Technical Conference and Exhibition.
Birkholzer, J., Zhou, Q., Cortis, A., Finsterle, S., 2011. A sensitivity study on regional pressure buildup from large-scale CO_2 storage projects. Energy Procedia 4, 4371–4378.
Blaskovich, F., Cain, G., Sonier, F., Waldren, D., Webb, S., 1983. A multicomponent isothermal system for efficient reservoir simulation. Middle East Oil Technical Conference and Exhibition.
Carey, J.W., 2013. Geochemistry of wellbore integrity in CO_2 sequestration: portland cement-steel-brine-CO_2 interactions. Rev. Mineral. Geochem. 77, 505–539.
Carey, J.W., Svec, R., Grigg, R., Lichtner, P.C., Zhang, J., Crow, W., 2009. Wellbore integrity and CO_2-brine flow along the casing-cement microannulus. Energy Procedia 1,

3609–3615.
Carey, J.W., Svec, R., Grigg, R., Zhang, J., Crow, W., 2010. Experimental investigation of wellbore integrity and CO_2–brine flow along the casing–cement microannulus. Int. J. Greenh. Gas Control. 4, 272–282.
Carlson, F.M., 1981. Simulation of relative permeability hysteresis to the nonwetting phase. SPE Annual Technical Conference and Exhibition.
Carroll, S., Carey, J.W., Dzombak, D., Huerta, N.J., Li, L., Richard, T., Um, W., Walsh, S.D., Zhang, L., 2016. Role of chemistry, mechanics, and transport on well integrity in CO_2 storage environments. Int. J. Greenh. Gas Control. 49, 149–160.
Chen, H., Onishi, T., Olalotiti-Lawal, F., Datta-Gupta, A., 2018. Streamline tracing and applications in naturally fractured reservoirs using embedded discrete fracture models. SPE Annual Technical Conference and Exhibition.
Clochard, V., DeVault, B., Bowen, D., Wangkawong, K., Delepine, N., 2018. Quadri-joint Inversion: Method and Application to the Big Sky 9C 3D Dataset in Northern Montana, Interpretation.
Corey, A.T., 1954. The interrelation between gas and oil relative permeabilities. Producers Monthly 19, 38–41.
Crow, W., Carey, J.W., Gasda, S., Williams, D.B., Celia, M., 2010. Wellbore integrity analysis of a natural CO_2 producer. Int. J. Greenh. Gas Control. 4, 186–197.
Dahle, H.K., Eigestad, G.T., Nordbotten, J.M., Pruess, K., 2009. A Model-oriented Benchmark Problem for CO_2 Storage, Workshop on Modeling and Risk of Assessment of Geological Storage of CO_2.
Dai, Z., Stauffer, P.H., Carey, J.W., Middleton, R.S., Lu, Z., Jacobs, J.F., Hnottavange-Telleen, K., Spangler, L.H., 2014. Pre-site characterization risk analysis for commercial-scale carbon sequestration. Environ. Sci. Technol. 48, 3908–3915.
Deng, H., Stauffer, P.H., Dai, Z., Jiao, Z., Surdam, R.C., 2012. Simulation of industrial-scale CO_2 storage: multi-scale heterogeneity and its impacts on storage capacity, injectivity and leakage. Int. J. Greenh. Gas Control. 10, 397–418.
Deutsch, C.V., Journel, A.G., 1998. GSLIB: Geostatistical Software Library and User"s Guide, second edition. Oxford University Press, Oxford, UK.
Fakcharoenphol, P., Kurtoglu, B., Kazemi, H., Charoenwongsa, S., Wu, Y.-S., 2014. The effect of osmotic pressure on improve oil recovery from fractured shale formations. SPE Unconventional Resources Conference.
Fenghour, A., Wakeham, W.A., Vesovic, V., 1998. The viscosity of carbon dioxide. J. Phys. Chem. Ref. Data 27, 31–44.
Firoozabadi, A., Hauge, J., 1990. Capillary Pressure in Fractured Porous Media (includes associated papers 21892 and 22212). J. Pet. Technol. 42, 784–791.
Fourar, M., Bories, S., Lenormand, R., Persoff, P., 1993. Two-phase flow in smooth and rough fractures: Measurement and correlation by porous-medium and pipe flow models. Water Resour. Res. 29, 3699–3708.
Friedman, J.H., 1991. Adaptive spline networks. Adv. Neural Inf. Process. Syst. 675–683.
Harp, D.R., Pawar, R., Carey, J.W., Gable, C.W., 2016. Reduced order models of transient CO_2 and brine leakage along abandoned wellbores from geologic carbon sequestration reservoirs. Int. J. Greenh. Gas Control. 45, 150–162.
Hill, M.C., 2000. Methods and guidelines for effective model calibration. Building Partnerships 1–10.
Hu, L., Pan, L., Zhang, K., 2012. Modeling brine leakage to shallow aquifer through an open wellbore using T2WELL/ECO2N. Int. J. Greenh. Gas Control. 9, 393–401.
Hyman, J.D., Karra, S., Makedonska, N., Gable, C.W., Painter, S.L., Viswanathan, H.S., 2015. dfnWorks: a discrete fracture network framework for modeling subsurface flow and transport. Comput. Geosci. 84, 10–19.
Iino, A., Arihara, N., 2007. Use of streamline simulation for waterflood management in naturally fractured reservoirs. International Oil Conference and Exhibition in Mexico.
Iino, A., Onishi, T., Olalotiti-Lawal, F., Datta-Gupta, A., 2018. Rapid Field-scale Well spacing optimization in tight and shale oil reservoirs using fast marching method. Unconventional Resources Technology Conference (URTec).
Iman, R.L., Conover, W., 1980. Small sample sensitivity analysis techniques for computer models. With an application to risk assessment. Commun. Statist. Theory Methods 9, 1749–1842.
Jordan, A.B., Stauffer, P.H., Harp, D., Carey, J.W., Pawar, R.J., 2015. A response surface model to predict CO_2 and brine leakage along cemented wellbores. Int. J. Greenh. Gas Control. 33, 27–39.
Juanes, R., Spiteri, E., Orr, F., Blunt, M., 2006. Impact of relative permeability hysteresis on geological CO_2 storage. Water Resour. Res. 42.
Kazemi, H., Merrill Jr, L., Porterfield, K., Zeman, P., 1976. Numerical simulation of water-oil flow in naturally fractured reservoirs. Old Spe J. 16, 317–326.
Keating, E.H., Fessenden, J., Kanjorski, N., Koning, D.J., Pawar, R., 2010. The impact of CO_2 on shallow groundwater chemistry: observations at a natural analog site and implications for carbon sequestration. Environ. Earth Sci. 60, 521–536.
Killough, J., 1976. Reservoir simulation with history-dependent saturation functions. Old Spe J. 16, 37–48.
King, S., 2016. Reservoir Reduced-Order-Model-Generator (RROM-Gen) Tool User"s Manual. Version: 2016.11-1.2. .
Kirk, K.B., 2002. A Preliminary Investigation of the Madison Aquifer for a Drinking Water Supply in Bozeman, Montana. Montana State University-Bozeman, College of Letters & Science.
Krevor, S., Blunt, M.J., Benson, S.M., Pentland, C.H., Reynolds, C., Al-Menhali, A., Niu, B., 2015. Capillary trapping for geologic carbon dioxide storage–From pore scale physics to field scale implications. Int. J. Greenh. Gas Control. 40, 221–237.
Land, C.S., 1968. Calculation of imbibition relative permeability for two-and three-phase flow from rock properties. Old Spe J. 8, 149–156.
Lee, J., 1982. Well Testing. Society of Petroleum Engineers., New York.
Li, L., Lee, S.H., 2006. Efficient field-scale simulation for black oil in a naturally fractured reservoir via discrete fracture networks and homogenized media. International Oil & Gas Conference and Exhibition in China.
Li, Boxiao., Tchelepi, Hamdi A., Benson, Sally M., 2013. The influence of capillary entry-pressure representation on CO_2 solubility trapping. Energy Procedia 37, 3808–3815.
Li, B., Bhark, E.W., Gross, S.J., Billiter, T.C., Dehghani, K., 2018. Best practices of assisted history matching using design of experiments. SPE Annual Technical Conference and Exhibition.
Lim, K., Aziz, K., 1995. Matrix-fracture transfer shape factors for dual-porosity simulators. J. Pet. Sci. Eng. 13, 169–178.
Lupe, R., Ahlbrandt, T.S., 1975. Sandstone Geometry, Porosity and Permeability Distribution, and Fluid Migration in Eolian System Reservoirs. US Geological Survey.
Mathias, S.A., Hardisty, P.E., Trudell, M.R., Zimmerman, R.W., 2009. Approximate solutions for pressure buildup during CO_2 injection in brine aquifers. Transp. Porous Media 79, 265–284.
Mathias, S.A., Gluyas, J.G., González Martínez de Miguel, G.J., Hosseini, S.A., 2011. Role of partial miscibility on pressure buildup due to constant rate injection of CO_2 into closed and open brine aquifers. Water Resour. Res. 47.
McKay, M.D., Beckman, R.J., Conover, W.J., 1979. Comparison of three methods for selecting values of input variables in the analysis of output from a computer code. Technometrics 21, 239–245.
Metz, B., Davidson, O., De Coninck, H., Loos, M., Meyer, L., 2005. IPCC special report on carbon dioxide capture and storage. Intergovernmental Panel on Climate Change, Geneva (Switzerland). Working Group III.
Mijic, A., LaForce, T.C., Muggeridge, A.H., 2014. CO_2injectivity in saline aquifers: The impact of non-Darcy flow, phase miscibility, and gas compressibility. Water Resour. Res. 50, 4163–4185.
Monteagudo, J., Firoozabadi, A., 2004. Control-volume method for numerical simulation of two-phase immiscible flow in two-and three-dimensional discrete-fractured media. Water Resour. Res. 40.
Nguyen, M., Onishi, T., Carey, J.W., Will, B., Zaluski, W., Bowen, D., DeVault, B., Duguid, A., Spangler, L., Stauffer, P.H., 2017a. Risk Assessment of Carbon Sequestration Into a Naturally Fractured Reservoir at Kevin Dome, Montana. Los Alamos National Lab. (LANL), Los Alamos, NM (United States).
Nguyen, M.C., Zhang, X., Wei, N., Li, J., Li, X., Zhang, Y., Stauffer, P.H., 2017b. An object-based modeling and sensitivity analysis study in support of CO_2 storage in deep saline aquifers at the Shenhua site, Ordos Basin. Geomech. Geophys. Geo-energy Geo-resources 3 (3), 293–314.
Nguyen, M.C., Zhang, Y., Li, J., Li, X., Bai, B., Wu, H., Wei, N., Stauffer, P.H., 2017c. A geostatistical study in support of CO_2 storage in deep saline aquifers of the Shenhua CCS project, Ordos Basin, China. Energy Procedia 114, 5826–5835.
Noorishad, J., Mehran, M., 1982. An upstream finite element method for solution of transient transport equation in fractured porous media. Water Resour. Res. 18, 588–596.
Nordbotten, J.M., Celia, M.A., Bachu, S., Dahle, H.K., 2005. Semianalytical solution for CO_2 leakage through an abandoned well. Environ. Sci. Technol. 39, 602–611.
Nordbotten, J.M., Kavetski, D., Celia, M.A., Bachu, S., 2008. Model for CO_2 leakage including multiple geological layers and multiple leaky wells. Environ. Sci. Technol. 43, 743–749.
Oh, J., Kim, K.-Y., Han, W.S., Kim, T., Kim, J.-C., Park, E., 2013. Experimental and numerical study on supercritical CO_2/brine transport in a fractured rock: implications of mass transfer, capillary pressure and storage capacity. Adv. Water Resour. 62, 442–453.
Olalotiti-Lawal, F., 2018. Effective Reservoir Management for Carbon Utilization and Storage Applications. Doctoral Dissertation. Texas A&M University.
Olalotiti-Lawal, F., Onishi, T., Datta-Gupta, A., Fujita, Y., Hagiwara, K., 2017. Post-Combustion CO_2 EOR Development in a Mature Oil Field: Model Calibration Using a Hierarchical Approach, SPE Annual Technical Conference and Exhibition. Society of Petroleum Engineers.
Olalotiti-Lawal, F., Onishi, T., Datta-Gupta, A., Fujita, Y., Watanabe, D., Hagiwara, K., 2018. Post-Combustion CO_2 WAG Pilot in a Mature Field: Model Calibration and Optimization, SPE Annual Technical Conference and Exhibition. Society of Petroleum Engineers.
Onishi, T., Stauffer, P.H., Nguyen, M., Carey, J.W., 2017. Big Sky Project Preliminary Results June 28, 2017. Los Alamos National Lab. (LANL), Los Alamos, NM (United States).
Pawar, R., Carey, J., Chipera, S., Fessenden, J., Kaszuba, J., Keating, G., Lichtner, P., Olsen, S., Stauffer, P., Viswanathan, H., 2006. Development of a framework for long-term performance assessment of geologic CO_2 sequestration sites. Eighth Int. Conf. Greenh. Gas Control Technol. (GHGT-8) 19–22.
Pawar, R.J., Bromhal, G.S., Chu, S., Dilmore, R.M., Oldenburg, C.M., Stauffer, P.H., Zhang, Y., Guthrie, G.D., 2016. The National Risk Assessment Partnership's integrated assessment model for carbon storage: a tool to support decision making amidst uncertainty. Int. J. Greenh. Gas Control. 52, 175–189.
Pham, T., Maast, T., Hellevang, H., Aagaard, P., 2011. Numerical modeling including hysteresis properties for CO_2 storage in Tubåen formation, Snøhvit field, Barents Sea. Energy Procedia 4, 3746–3753.
Pieters, D., Graves, R., 1994. Fracture relative permeability: linear or non-linear function of saturation. International Petroleum Conference and Exhibition of Mexico.
Pruess, K., Garcia, J., 2002. Multiphase flow dynamics during CO_2 disposal into saline aquifers. Environ. Geol. 42, 282–295.
Pruess, K., Oldenburg, C., Moridis, G., 1999. TOUGH2 user's guide version 2. Lawrence Berkeley National Laboratory.
Redlich, O., Kwong, J.N., 1949. On the thermodynamics of solutions. V. An Equation of State. Fugacities of Gaseous Solutions. Chem. Rev. 44, 233–244.
Remy, N., 2004. Geostatistical Earth Modeling Software: User's Manual.
Romm, E., 1966. Flow characteristics of fractured rocks. Nedra, Moscow 283.
Spycher, N., Pruess, K., 2005. CO_2-H_2O mixtures in the geological sequestration of CO_2. II. Partitioning in chloride brines at 12–100 C and up to 600 bar. Geochim. Cosmochim. Acta 69, 3309–3320.

Spycher, N., Pruess, K., 2010. A phase-partitioning model for CO_2–brine mixtures at elevated temperatures and pressures: application to CO_2-enhanced geothermal systems. Transp. Porous Media 82, 173–196.
Stauffer, P.H., Viswanathan, H., Pawar, R.J., Klasky, M.L., Guthrie, G.D., 2006. CO_2-PENS: a CO_2 sequestration systems model supporting risk-based decisions. Proceedings of the 16th International Conference on Computational Methods in Water Resources. pp. 19–22.
Stauffer, P.H., Viswanathan, H.S., Pawar, R.J., Guthrie, G.D., 2009. A system model for geologic sequestration of carbon dioxide. Environ. Sci. Technol. 43 (3), 565–590.
Stauffer, P.H., Pawar, R.J., Surdam, R.C., Jiao, Z., Deng, H., Lettelier, B.C., Viswanathan, H.S., Sanzo, D.L., Keating, G.N., 2011. Application of the CO_2-PENS risk analysis tool to the Rock Springs Uplift, Wyoming. Energy Procedia 4, 4084–4091.
Stauffer, P.H., Dai, Z., Lu, Z., Middleton, R.S., Jacobs, J.F., Carey, J.W., 2013. LANL Deliverable to the Big Sky Carbon Sequestration Partnership: Preliminary CO_2-PENS Model. Los Alamos National Laboratory (LANL).
Stauffer, P.H., Shaoping, C., Cameron, T., Pawar, R.J., 2016. NRAP Intergrated Assessment Model-Carbon Storage (NRAP-IAM-CS) Tool User's Manual. Version: 2016.04-1.1. .
Thayer, P.A., 1983. Relationship of Porosity and Permeability to Petrology of the Madison Limestone in Rock Cores from Three Test Wells in Montana and Wyoming.
Trautz, R.C., Pugh, J.D., Varadharajan, C., Zheng, L., Bianchi, M., Nico, P.S., Spycher, N.F., Newell, D.L., Esposito, R.A., Wu, Y., 2012. Effect of dissolved CO_2 on a shallow groundwater system: a controlled release field experiment. Environ. Sci. Technol. 47, 298–305.
Van Genuchten, M.T., 1980. A closed-form equation for predicting the hydraulic conductivity of unsaturated soils. Soil Sci. Soc. Am. J. 44, 892–898.
Vasco, D.W., Datta-Gupta, A., 2016. Subsurface Fluid Flow and Imaging: With Applications for Hydrology, Reservoir Engineering, and Geophysics. Cambridge University Press.
Vesovic, V., Wakeham, W., Olchowy, G., Sengers, J., Watson, J., Millat, J., 1990. The transport properties of carbon dioxide. J. Phys. Chem. Ref. Data 19, 763–808.
Vilarrasa, V., Carrera, J., Bolster, D., Dentz, M., 2013. Semianalytical solution for CO_2 plume shape and pressure evolution during CO_2 injection in deep saline formations. Transp. Porous Media 97, 43–65.
Viswanathan, H.S., Pawar, R.J., Stauffer, P.H., Kaszuba, J.P., Carey, J.W., Olsen, S.C., Keating, G.N., Kavetski, D., Guthrie, G.D., 2008. Development of a hybrid process and system model for the assessment of wellbore leakage at a geologic CO_2 sequestration site. Environ. Sci. Technol. 42, 7280–7286.
Vuke, S.M., Porter, K.W., Lonn, J.D., Lopez, D.A., 2007. Geologic Map of Montana: Montana Bureau of Mines and Geology Geologic Map 62-A, 73 p. 2 sheets, scale, pp. 1 500,000.
Warren, J., Root, P.J., 1963. The behavior of naturally fractured reservoirs. Old Spe J. 3, 245–255.
White, M., Oostrom, M., Lenhard, R., 1995. Modeling fluid flow and transport in variably saturated porous media with the STOMP simulator. 1. Nonvolatile three-phase model description. Adv. Water Resour. 18, 353–364.
Wilkin, R.T., DiGiulio, D.C., 2010. Geochemical impacts to groundwater from geologic carbon sequestration: controls on pH and inorganic carbon concentrations from reaction path and kinetic modeling. Environ. Sci. Technol. 44, 4821–4827.
Wu, Y.-S., Pan, L., Pruess, K., 2004. A physically based approach for modeling multiphase fracture–matrix interaction in fractured porous media. Adv. Water Resour. 27, 875–887.
Yoshida, N., Levine, J.S., Stauffer, P.H., 2016. Investigation of uncertainty in CO_2 reservoir models: a sensitivity analysis of relative permeability parameter values. Int. J. Greenh. Gas Control. 49, 161–178.
Zhou, Q., 2013. Milestone Report: Summary of Site Characterization, Data Collection and Review. Development of Static Geologic Model, and Preliminary Multiphase Flow and Reactive Transport Modeling Activities.
Zhou, Q., Oldenburg, C.M., Spangler, L.H., Birkholzer, J.T., 2017. Approximate solutions for diffusive fracture-matrix transfer: Application to storage of dissolved CO_2 in fractured rocks. Water Resour. Res. 53, 1746–1762.
Zyvoloski, G., 2007. FEHM: A Control Volume Finite Element Code for Simulating Subsurface Multi-phase Multi-fluid Heat and Mass Transfer. Los alamos unclassified report LA-UR-07-3359.